Detailed calculation of the thermoelectric figure of merit in an *n*-doped SiGe alloy

Iorwerth O. Thomas and G. P. Srivastava
School of Physics, University of Exeter, Stocker Road, Exeter EX4 4QL, United Kingdom
(Received 31 January 2012; revised manuscript received 27 June 2012; published 16 July 2012)

In this study, we develop a detailed numerical approach towards the theoretical calculation of the phonon contribution to the dimensionless figure of merit ZT that parameterizes the efficiency of the thermoelectric effect, and apply it to the case of an n-doped $Si_{0.754}Ge_{0.246}$ alloy sample. This is achieved by using accurate lattice dynamical eigensolutions from the application of the density functional perturbation theory, supplemented by a semiempirical approach for crystal anharmonicity. The success of the application of the theoretical method for lattice thermal conductivity, within the single-mode relaxation time scheme, in explaining available experimental data is highlighted. Using well-known phenomenological theories, based on the nearly-free electron model, for the behavior of the electronic components of ZT, we are then able to calculate the figure of merit over a temperature range of 300–1200 K.

DOI: 10.1103/PhysRevB.86.045205 PACS number(s): 72.20.Pa, 63.20.dk, 63.20.K−, 66.70.−f

I. INTRODUCTION

The concept of conversion of electricity into heat and vice versa—the thermoelectric effect—has been considered very useful for several decades (see, e.g., Refs. 1–4). This has recently been the subject of intense theoretical and experimental interest.[5,6] This interest has arisen largely since it has been shown experimentally that the efficiency of thermoelectric conversion (which is described by the figure of merit ZT) can be substantially increased with nanostructuring.[5–7] In general, existing three-dimensional thermoelectric (TE) materials are found to exhibit high efficiency ($ZT > 0.5$) either at low temperatures (such as Bi_2Te_3, between 200–500 K) or in an intermediate temperature range (such as PbTe, between 600–900 K), or at high temperatures (such as SiGe alloys, between 800–1300 K). It has also been suggested that it may soon be possible to engineer thermoelectric structures that function optimally across a wide variety of temperatures,[5] leading to obvious industrial applications. However, in order to properly engineer nanostructured TE materials, we must understand not only how nanostructuring affects the various parameters governing thermoelectric efficiency but which parameters produce the greatest effect. At present, it seems that approaches that attempt to minimize the phonon contribution to the thermal conductivity show most promise.[5,8] However, the theoretical behavior of this quantity is not currently well understood.

Over the past several decades, a large number of theoretical investigations have been undertaken in order to assess ZT of semiconductor single crystals. While the electronic properties are reasonably well formulated within the nearly-free-electron model, numerical calculations that fully account for the temperature variation of that most basic of quantities, viz., the Fermi energy E_F have not necessarily been made. The quantity that has remained the least well convincingly studied is the lattice contribution to thermal conductivity κ_{ph}. In this respect, four publications deserve to be mentioned. Meddins and Parrott[9] do not elaborate on any specific method for evaluating the electrical conductivity σ, Seebeck coefficient S and the bipolar contribution to thermal conductivity and resort to a high-temperature interpolative scheme for the calculation of κ_{ph} for SiGe alloys. Vining[10] has adopted a complete treatment for the electronic contributions, viz., for σ, S, electronic and bipolar contributions to thermal conductivity κ_{el} and κ_{bp}, respectively. However, this work does not explicitly consider the temperature dependence of E_F. Moreover, Vining has employed a phenomenologically derived, simple expression for the anharmonic phonon relaxation time, incorporating a low-temperature form of the three-phonon Umklapp scattering rate, where the three-phonon Normal scattering rate is taken to be a simple scaling (by an undeclared factor) of the Umklapp scattering rate. These low-temperature considerations should not be expected to be valid at high temperatures, entailing that an application of that scheme to systems of reduced dimensionality is unlikely to be useful. Similarly, the more recent work of Minnich *et al.*[11] improves on Vining's[10] and Slack and Hussein's[12] similar treatment of the electronic parameters of the system, but performs the phonon conductivity calculations using an approach similar to that used by Vining. Slack and Hussein[12] themselves use an empirical approach to the phonon conductivity. Hicks and Dresselhaus[8] have attempted to explicitly include the Fermi energy E_F in their formulation of σ and S, but did not account for its temperature variation. Although they have discussed the effects of reducing dimensionality on the various TE coefficients, in their treatment, κ_{ph} is considered to be no more than a temperature-independent adjustable parameter. Thus it seems reasonable to conclude that—to our knowledge—there is currently no publication that presents a systematic numerical calculation of the TE coefficients of semiconductors over a wide range of temperatures.[13]

In this paper, we aim to provide as complete and accurate a theoretical approach as possible to the calculation of the phonon contribution to the thermal conductivity (and hence to the calculation of ZT) in alloyed systems, which we hope will serve as a basis for future work performed on more complex, nanostructured systems.

In the next section of the paper, we shall outline the theoretical background of our calculation. Firstly, we discuss the behavior of the electronic components of ZT using the well-known expressions based on the nearly free-electron model for the electronic band structure. The behavior of these components is well understood in bulk materials—our

treatment of them will hence be phenomenological and a summary in nature, as it is the calculation of the contribution arising from phonons that is most challenging and which shall therefore command the majority of our attention. Next, we turn to our theoretical scheme for the computation of the lattice contribution to ZT, viz., the phonon conductivity. One important element in our approach that should be emphasized is that we make use of an expression for the anharmonic crystal potential that includes contributions from the optical as well as acoustic modes; this expression is defined in a semiempirical fashion, and we expect this approach to complement other, recently developed approaches such as those of Refs. 14–16. This will be discussed in more detail in the second section of the paper.

The third section details our approach for calculating the phonon eigenmodes, frequencies and velocities through the use of density functional perturbation theory (DFPT)[17] (reviewed in Ref. 18). In the fourth section, we detail the results of our study, beginning with the results of our fitting of the electronic parameters to the experimental data, and then, turning to the focus of this paper, we initiate our discussion of the phonon-dependent aspects of the sample with an examination of the form of the dispersion relations of the model cell used in the DFTP calculations and how they are affected by bond relaxation, and a discussion of some theoretical issues surrounding the notion of a "mean-free path" and its definition within the context of the study of thermal conductivity. Lastly, we discuss the results of our calculation of the total thermal conductivity and the figure of merit ZT and how they compare to the experimental results for ZT of sample 7 in Meddins and Parrott,[9] before summarizing our conclusions.

II. THEORETICAL BACKGROUND

As indicated above, a typical measure of the efficiency of thermoelectric conversion is given by the dimensionless figure of merit ZT, defined as follows:

$$ZT = \frac{S^2 \sigma T}{\kappa}, \tag{1}$$

where S is the Seebeck coefficient for the material, σ is its electrical conductivity, T its temperature, and κ is its total thermal conductivity. We can treat the thermal conductivity as a sum:

$$\kappa = \kappa_{\mathrm{el}} + \kappa_{\mathrm{ph}}, \tag{2}$$

where κ_{el} is the electronic and κ_{ph} is the phonon (lattice) contributions. Obviously, it is through the latter term that the phonon physics of the material affects the figure of merit. Following previous theoretical works,[8,10–12] we will evaluate σ, S, and κ_{el} within the application of the nearly-free electron model. We present an extensive theoretical approach for calculation of the lattice thermal conductivity κ_{ph}.

A. Electronic components of ZT

Firstly, we shall examine the behavior of the components of ZT, which are primarily electronic in nature (S, σ, κ_{el}), as a prelude to examining the more difficult phonon conductivity contribution κ_{ph}. Since we are more interested in the fine detail of the latter, our examination of the former is of necessity somewhat brief, being more concerned with suitable phenomenological modeling of the quantities in question as opposed to the minutiae of their physics. To this end, we shall discuss the application of our expressions to the relevant data in this section, so as not to detract from the main focus of our study.

1. Temperature variation of Fermi energy

Numerically accurate values of the Fermi energy are required at each temperature we wish to calculate the electronic transport coefficients. For the system under study, we use the following expression for the incompletely ionized, extrinsic semiconductors,[19] but replacing the first term with one more suited to the case of strongly degenerate semiconductors:[20]

$$E_F = \frac{(3\pi^2 N_{\mathrm{don}})^{2/3}}{2\hbar^2 (2N_{\mathrm{val}})^{2/3} m_e^{\mathrm{dos}}} + \frac{k_{\mathrm{B}} T}{2} \ln \frac{N_{\mathrm{don}}}{2A_e N_{\mathrm{val}}} - k_{\mathrm{B}} T \sinh^{-1}\left[\sqrt{\frac{A_e N_{\mathrm{val}}}{8N_{\mathrm{don}}}} e^{-(E_c - E_d)/2k_{\mathrm{B}}T}\right]. \tag{3}$$

Here, m_e^{dos} is the density-of-states effective mass and N_{val} is the number of valleys in the conduction band. We define $A_{e/h} = 2(m_{e/h}^{\mathrm{dos}/*} k_{\mathrm{B}} T/\hbar^2)^{3/2}$, and the quantity N_{don} represents the number of donor impurities.

2. Seebeck coefficient

We adopt the nearly free electron model and use the following expression for the absolute value of the Seebeck coefficient:[4]

$$|S| = \frac{k_{\mathrm{B}}}{e}\left[\mathcal{M}(\alpha) - \eta_R\right], \tag{4}$$

$$\mathcal{M}(y) = \frac{(s+2.5)}{(s+1.5)} \frac{\mathcal{F}_{s+3/2}(y)}{\mathcal{F}_{s+1/2}(y)}. \tag{5}$$

Here, $\alpha = \eta_R - (E_c/k_{\mathrm{B}}T)$, where $\eta_R = E_F/k_{\mathrm{B}}T$ with E_F being the Fermi energy, s is determined by the dominant electron scattering mechanism, and we make use of the Fermi integrals

$$\mathcal{F}_a(y) = \int \frac{x^a}{e^{x-y}+1} dx. \tag{6}$$

3. Electrical conductivity

We adopt the nearly-free electron model and write the expression for the conductivity derived in Drabble and Goldsmit,[21] generalized to the case of multiple valleys, as

$$\sigma = \frac{N_{\mathrm{val}} e^2 \tau_0}{3\pi^2 m_c^*} \left(\frac{2m_e^{\mathrm{dos}} k_{\mathrm{B}} T}{\hbar^2}\right) \left(p + \frac{3}{2}\right)^p \mathcal{F}_{p+1/2}(\alpha), \tag{7}$$

where N_{val} is the number of energy valleys, m_c^* is the conductivity effective mass, and τ_0 represents the energy-independent portion of the relaxation time

$$\tau = \tau_0 (\alpha k_{\mathrm{B}} T)^p, \tag{8}$$

with p being a constant depending on the type of scattering. We have considered ionized impurity (imp) scattering, acoustic phonon (ac) scattering, and optical phonon (op) scattering as being relevant to our work. Expressions for these scattering rates from each valley are[22]

$$\tau_{\text{imp}}^{-1} = \frac{Z^2 e^4 N_i C}{16\pi\epsilon^2 (2m^{\text{dos}})^{1/2} k_{\text{B}} T)^{3/2}} \alpha^{-3/2}, \tag{9}$$

$$\tau_{\text{ac}}^{-1} = \frac{\sqrt{2} E_D^2 m^{\text{dos}^{3/2}} (k_{\text{B}} T)^{3/2}}{\pi\hbar^4 \rho c_L^2} \alpha^{1/2}, \tag{10}$$

$$\tau_{\text{op}}^{-1} = \frac{(2m^{\text{dos}})^{3/2} D_o^2}{4\pi\hbar^3 \rho\omega_0} [(\bar{n}+1)\sqrt{(\alpha k_{\text{B}} T - \hbar\omega_0)} + \bar{n}\sqrt{(\alpha k_{\text{B}} T + \hbar\omega_0)}]. \tag{11}$$

In the above expressions, m_c^* is the conductivity effective mass, ρ is the density of the sample, c_L the speed of LA phonons, E_D is an acoustic deformation potential, ω_0 is the frequency of the highest longitudinal optical mode, D_o is an optical deformation parameter, ϵ is the host dielectric constant, Ze is the impurity charge, N_i is the impurity concentration, and C is a constant that is usually between 1.4 and 2.[22] The first and second terms in the optical scattering expression are contributions from phonon emission and absorption events, respectively. From the above expressions, it is clear that the parameter p takes values $3/2$ for impurity scattering and $-1/2$ for acoustic and optical phonon scattering. The conductivity expressions, considering individual scattering mechanisms, then become

$$\sigma_{\text{imp}} = \frac{64\sqrt{3} N_{\text{val}} \epsilon^2 \left(m_e^{\text{dos}}\right)^2}{\pi m_c^* Z^2 e^2 N_i C} \left(\frac{k_{\text{B}} T}{\hbar}\right)^3 \mathcal{F}_2(\alpha), \tag{12}$$

$$\sigma_{\text{ac}} = \frac{2 N_{\text{val}} e^2 \hbar \rho c_L^2}{3\pi E_D^2 m_c^*} \mathcal{F}_0(\alpha), \tag{13}$$

$$\sigma_{\text{op}} = \begin{cases} \sigma_{\text{op, ab}} & E \leqslant \hbar\omega_0 \\ \sigma_{\text{op, ab}} + \sigma_{\text{op, em}} & E > \hbar\omega_0 \end{cases}, \tag{14}$$

$$\sigma_{\text{op, ab}} = \frac{4 N_{\text{val}} e^2 \rho\omega_0 k_{\text{B}} T}{3\pi D_o^2 \bar{n} m_c^*} \mathcal{F}_0(\alpha), \tag{15}$$

$$\sigma_{\text{op, em}} = \frac{4 N_{\text{val}} e^2 \rho\omega_0 k_{\text{B}} T}{3\pi D_o^2 (\bar{n}+1) m_c^*} \mathcal{F}_0(\alpha). \tag{16}$$

Using Matthiessen's rule, we sum the resistivity contributions as follows:

$$\sigma_n^{-1} = \sigma_{\text{ac}}^{-1} + \sigma_{\text{op}}^{-1} + \sigma_{\text{imp}}^{-1}. \tag{17}$$

We denote the conductivity as σ_n since it is the electronic contribution to the conductivity. For our system, and in the temperature range of interest (i.e., above 300 K), the impurity and optical phonon scattering rates are found, respectively, to be approximately four and two orders of magnitude smaller than the acoustic phonon scattering rate. We thus considered only the dominant acoustic contribution and neglected the others. We remark that there also exists a small contribution to the conductivity from holes, which we denote σ_p, and model in a simple fashion described later in this paper. This last does not significantly contribute to the overall conductivity, which is dominated by σ_n, however, it will prove important when considering the bipolar contribution to the thermal conductivity, which we discuss next.

4. *Electronic and bipolar contributions to thermal conductivity*

The electronic contribution to the thermal conductivity is typically taken to be $\kappa_{\text{el}} \propto \sigma_e T$, with the Lorentz number $\mathcal{L}$ being the constant of proportionality (see, for example, Refs. 19,21, and 23). However, a complication arises when we deal with the behavior of the system at high temperatures, which require an account of the effects of thermally excited holes. The thermal conductivity contributions arising from electrons and holes are not simply additive; in combination they give rise to an additional contribution known as the *bipolar* term,[2,21,23–25] which may be quite large even if σ_h/σ_n is small. Following the derivation given in Ref. 21, we may write the total electronic conductivity (including this term) as

$$\kappa_{\text{el}} = \frac{k_{\text{B}}^2}{e^2} \left\{ \mathcal{L}(\alpha)\sigma_n T + \mathcal{L}(\beta)\sigma_p T + \frac{\sigma_n \sigma_p T}{\sigma} \left[\frac{(E_c - E_v)}{k_{\text{B}} T} + \mathcal{M}(\alpha) + \mathcal{M}(\beta) \right]^2 \right\},$$
$$\mathcal{L}(y) = \frac{(s+3.5)(s+1.5)\mathcal{F}_{s+5/2}(y)\mathcal{F}_{s+1/2}(y) - (s+2.5)^2 \mathcal{F}_{s+3/2}(y)^2}{(s+1.5)^2 \mathcal{F}_{s+1/2}(y)^2}, \tag{18}$$

where we have defined $\beta = (E_v/k_{\text{B}}T) - \eta_R$.

The hole density can be written as $n_h \approx n_{\text{in}}^2/N_{\text{don}}$,[19] where $n_{\text{in}} = \sqrt{A_e A_h} \exp[-(E_c - E_v)/2k_{\text{B}}T]$, allowing us to make use of the following simplified expression:

$$\sigma_p = eG \exp[-(E_c - E_v)/k_{\text{B}}T], \tag{19}$$

with G treated as an adjustable parameter.

B. Phonon contribution to thermal conductivity

Here, we move the focus of our discussion to the theoretical heart of our work: the calculation of the lattice (phonon) portion κ_{ph} of the thermal conductivity κ. Working within the single-mode relaxation time approximation,[26] we write the following expression for the thermal conductivity:

$$\kappa_{\text{ph}} = \frac{\hbar^2}{3V k_{\text{B}} T^2} \sum_{\boldsymbol{q}s} c_s^2(\boldsymbol{q}) \omega^2(\boldsymbol{q}s) \tau(\boldsymbol{q}s) \bar{n}_{\boldsymbol{q}s} (\bar{n}_{\boldsymbol{q}s} + 1)$$
$$= \sum_{\boldsymbol{q}s} \kappa_{\boldsymbol{q}s}, \tag{20}$$

where the total volume of the system is $V = N_{\text{cell}}\Omega_0$ (N_{cell} being the number of unit cells in the system and Ω_0 being the volume of each unit cell), $\boldsymbol{q}$ being the phonon wave vector, s

is the label of the phonon branch, $c_s(\boldsymbol{q})$ is the magnitude of the velocity for a given mode $\boldsymbol{q}s$, $\omega(\boldsymbol{q}s)$ is the frequency, and $\bar{n}_{\boldsymbol{q}s}$ is the Bose-Einstein distribution at equilibrium. The total single-mode relaxation time $\tau(\boldsymbol{q}s)$ is given by

$$\tau^{-1}(\boldsymbol{q}s) = \tau_{\mathrm{BD}}^{-1}(\boldsymbol{q}s) + \tau_{\mathrm{MD}}^{-1}(\boldsymbol{q}s) + \tau_{\mathrm{EP}}^{-1}(\boldsymbol{q}s) + \tau_{\mathrm{AH}}^{-1}(\boldsymbol{q}s), \quad (21)$$

where we have contributions from boundary scattering $\tau_{\mathrm{BD}}(\boldsymbol{q}s)$, mass-defect effects $\tau_{\mathrm{MD}}(\boldsymbol{q}s)$, electron-phonon interactions τ_{EP}, and anharmonic phonon-phonon interactions τ_{AH}. We shall discuss the first three contributions separately from the latter.

1. Harmonic scattering processes

The boundary scattering of phonons is expressed as[26]

$$\tau_{\mathrm{BD}}^{-1}(\boldsymbol{q}s) = \frac{c_s(\boldsymbol{q})}{L}, \quad (22)$$

where L is a measure of the effective size of the crystallite microstructure in the sample studied in Ref. 9. Mass-defect scattering arises due to the perturbation in crystal potential from the difference between the average mass of the alloy and the actual mass at a given atomic site of a particular species or isotope. We use the form given in Ref. 27,

$$\tau_{\mathrm{MD}}^{-1}(\boldsymbol{q}s) = \frac{\omega^2(\boldsymbol{q}s) g_s(\omega) P N_{\mathrm{cell}}}{4\pi} \Gamma_{\mathrm{MD}}, \quad (23)$$

where $g_s(\omega)$ is the phonon density of states and P is an adjustable parameter that we have introduced in the manner of Ref. 28 in order to absorb the effects of defects such as impurities and vacancies into $\tau_{\mathrm{MD}}(\boldsymbol{q}s)$, which are otherwise hard to parameterise. Γ_{MD} determines the average effect of species and isotope masses on the relaxation time. We use the formulation in Ref. 29, which incorporates both alloying and isotope effects in a relatively simple fashion, and express it for the alloy $\mathrm{Si}_x\mathrm{Ge}_{1-x}$ as

$$\Gamma_{\mathrm{MD}} = x\left(\frac{m_{\mathrm{Si}}}{\bar{m}}\right)^2 \Gamma_{\mathrm{IS}}(\mathrm{Si}) + (1-x)\left(\frac{m_{\mathrm{Ge}}}{\bar{m}}\right)^2 \Gamma_{\mathrm{IS}}(\mathrm{Ge}). \quad (24)$$

Here, m_{S} is the average mass of the species S, $\bar{m}$ is the average mass of the alloy constituents, and $\Gamma_{\mathrm{IS}}(\mathrm{S})$ incorporates the effects of the different isotope masses

$$\Gamma_{\mathrm{IS}}(\mathrm{S}) = \sum_i f_i \left(\frac{m_i - m_{\mathrm{S}}}{m_{\mathrm{S}}}\right)^2, \quad (25)$$

where m_i is the mass of the ith isotope and f_i its frequency. We use isotope data from Ref. 30 for Ge and from Ref. 31 for Si.

We parameterize the electron-phonon scattering through a generalization of the expression for medium-high doping used in Ref. 9:

$$\tau_{\mathrm{EP}}^{-1}(\boldsymbol{q}s) = \frac{n_{\mathrm{e}}\beta_1 \left|E_{\mathrm{def}}^s\right|^2 \sqrt{\pi\alpha_1} e^{-\alpha_1}}{\hbar\rho c_s(\boldsymbol{q})^2}. \quad (26)$$

Here, ρ is the density of the system, $\alpha_1 = m_e^* c_s(\boldsymbol{q}s)^2/2k_{\mathrm{B}}T$ and $\beta_1 = \hbar\omega(\boldsymbol{q}s)/k_{\mathrm{B}}T$, and we approximate n_{e} with N_{don}. E_{def} is the deformation potential, expressed as[26]

$$E_{\mathrm{def}}^s = A \sum_i^{N_{\mathrm{at}}} \hat{q} \cdot \boldsymbol{e}_{\boldsymbol{q}s}^i. \quad (27)$$

In this expression, $\mathbf{e}_{\boldsymbol{q}s}^i$ is a member of the set of N_{at} eigenvectors of an acoustic phonon mode $\boldsymbol{q}s$, N_{at} is the number of atoms in the unit cell, and A is an empirically adjustable parameter that controls the strength of the deformation potential and thus determines the magnitude of the electron-phonon scattering. Since this expression is only valid for acoustic phonons, in our numerical calculations, we set it equal to zero when the frequency corresponding to a mode $(\boldsymbol{q}s)$ is greater than some cutoff value corresponding to the largest value of an acoustic frequency at the Brillouin zone boundary (in our case, this is 170 cm^{-1}, which is the largest value at the X point in the z direction).

2. Anharmonic scattering processes

The calculation of the anharmonic contribution to the phonon relaxation time is far from simple. The behavior of this aspect of the system is determined by the values of the third-order force constants, whose effects can be summarized through a number of parameters such as the mode-dependent Grüneisen constants (γ_{MD}), which determine the strength of the scattering for different three-phonon processes.[26] One might think that the *ab initio* calculation of the third-order constants using DFPT methods such as those described in Refs. 18 and 32 or the force-displacement approach of Ref. 33 would be sufficient unto themselves, but there are a number of caveats that suggest that these approaches may be complemented by others such as the one employed in this paper.

Firstly, Lopuszyński and Majewski[34] have shown that in the elastic limit, *ab initio* calculations carried out via the theory of nonlinear elasticity show that while values of γ_{MD} for longitudinal acoustic (LA) modes are in reasonable agreement with experiment with discrepancies of around 0.9 to 10%, the difference between experimental and theoretical values of the transverse acoustic (TA) modes can be between roughly 84% to 98%. They suggest that this could be an indication that the final value of γ_{MD} is very sensitive to numerical errors in the third-order elastic constants on which it depends. Something similar could be true in the case of *ab initio* calculations performed outside of elastic limit, for in their recent, state-of-the-art calculation Esfarjani, Chen, and Stokes[16] employ the method of Ref. 33 in order to calculate force-constants *ab initio* and find that the values of the TA modes are again rather different from experiment due to a truncation in the number of third-order force constants used (they note that a large number are needed in order to calculate these modes correctly). While we are not presently aware of any calculations of the various γ_{MD} for the method of Ref. 32, on the strength of the foregoing one should perhaps avoid assuming unreservedly that an *ab initio* DFPT calculation will exactly reproduce the values of quantities that may be very sensitive to numerical error.

A further interesting issue is the temperature dependence of the γ_{MD} and their constituent force constants; if we examine the experimental behavior of the *mode-averaged* Grüneisen constant γ in Si and Ge in Figs. 61 and 51 on p. 373 and p. 413, respectively, of Ref. 35, we can see a rather strong temperature dependence as T is increased from 0 K to around 300 K, with γ decreasing from a positive value to a negative minimum before increasing once more and finally tending towards a positive value that is not necessarily identical to the

value close to $T = 0$ K. This implies that the behavior of the $\gamma_{\rm MD}$ is also temperature dependent, something that can also be inferred from measurements of the temperature dependence of the linear expansion constants[36] from which $\gamma_{\rm MD}$ may be derived. However, DFT and DFPT calculations are carried out at $T = 0$ K and do not give the behavior of the force constants as temperature is varied. Studies of the lattice heat transport in Si,[14,16] Ge,[14] and SiGe alloys[15] *do* give experimentally compatible values for various temperature ranges (see Ref. 14 for the entirety of the $T = 0$–300 K range, Ref. 16 for $T = 100$–500 K, and Ref. 15 for $T = 300$–600 K), and that deviations from experiment outside of those ranges may be accounted for by additional scattering effects as discussed in Ref. 16 for their results; but these studies contain no discussion of the effects of temperature on the force constants. One exception to this is Ward and Broido's *ab initio* examination of phonon relaxation times in Si and Ge,[37] where the effects of temperature on lattice properties via thermal expansion have been tested by varying the lattice constant by an amount appropriate for the temperature. They find that this gives results for the overall thermal conductivity that are within 1–2% of the value calculated using the $T = 0$ K force constants. It should be observed that the assumption that phonon properties are affected only by thermal expansion as temperature is varied is a product of the quasiharmonic approximation,[18,26,38] but since this approximation seems to be assumed valid in many calculations of this type (including the one in this paper) any problems arising from it are unlikely to be unique to their work.

That the aforementioned calculations work so well in spite of the potential problems we have raised is perhaps due to the complexity of the anharmonic contribution to the properties of the systems of interest. Simply put, it is difficult to tell how the individual mode contributions to each allowed three-phonon scattering event sum or cancel, since there are so many, and it is possible that much of the detailed variation due to error or temperature may be counteracted by their weighting as they enter into the calculation of the relaxation time. It is hard to tell at this point; perhaps more work is needed. This complexity also renders the calculations somewhat opaque to theoretical analysis despite their accuracy, and hence there is still much need for an approach to anharmonic and similar effects that is intermediate between that of a full *ab initio* approach and traditional long-wavelength limit calculations.

In future work, we intend to examine how lattice scattering is modified due to the properties of various nanostructures and, consequently, how the thermal conductivity (and therefore ZT) are affected by this modification. A full calculation would probably work against our aim of understanding the mechanisms involved since the complexity of the anharmonic contributions to systems in question might obscure the major details of the underlying mechanisms, and so we choose a semiempirical approach that employs *ab initio* DFPT elements, which we hope will capture as many of these factors as possible. The price we pay is the loss of a certain amount of predictive power regarding a given system; however, the prize we gain is that it becomes relatively simple to predict the effects of changes in structure *between* systems and account for the mechanisms underlying them, while in addition (hopefully) attaining good qualitative estimates of the magnitude of these effects. However, to begin with, we here test our approach using as detailed a calculation of the lattice contribution to the thermal conductivity as possible for a known system where experimental results are available, not only for reasons of simple validation, but because it gives an idea of plausible semiempirical parameter ranges suitable for cases of nanostructured systems of similar composition where appropriate experimental results may not yet be available.

The approach we have chosen is developed from the concepts presented in Refs. 26,39, and 40. In brief, we describe the anharmonic phonon-phonon scattering through the use of a continuum model to treat acoustic as well as optical phonon modes, and express the three-phonon scattering strength using the *mode-averaged* Grüneisen's constant γ, which we treat as a semiempirical adjustable parameter that can also be made temperature dependent if desired. The relevant expression for phonon anharmonic relaxation time in this approach is

$$\begin{aligned}\tau_{\rm AH}^{-1}(\boldsymbol{q}s) = {} & \frac{\pi\hbar\bar{\gamma}^2}{\rho V}\sum_{\boldsymbol{q}'s',\,\boldsymbol{q}''s'',\,\boldsymbol{G}}\frac{(\mathcal{B}_{\boldsymbol{q}s,\,\boldsymbol{q}'s',\,\boldsymbol{q}''s''})^2}{\omega(\boldsymbol{q}s)\omega(\boldsymbol{q}'s')\omega(\boldsymbol{q}''s'')} \\ & \times\Bigg[\frac{\bar{n}_{\boldsymbol{q}'s'}(\bar{n}_{\boldsymbol{q}''s''}+1)}{(\bar{n}_{\boldsymbol{q}s}+1)}\delta(\omega(\boldsymbol{q}s)+\omega(\boldsymbol{q}'s') \\ & -\omega(\boldsymbol{q}''s''))\delta_{\boldsymbol{q}+\boldsymbol{q}',\,\boldsymbol{q}''+\boldsymbol{G}}+\frac{1}{2}\frac{\bar{n}_{\boldsymbol{q}'s'}\bar{n}_{\boldsymbol{q}''s''}}{\bar{n}_{\boldsymbol{q}s}}\delta(\omega(\boldsymbol{q}s) \\ & -\omega(\boldsymbol{q}'s')-\omega(\boldsymbol{q}''s''))\delta_{\boldsymbol{q}+\boldsymbol{G},\,\boldsymbol{q}'+\boldsymbol{q}''}\Bigg],\end{aligned} \tag{28}$$

where

$$\begin{aligned}\mathcal{B}_{i,j,k} = {} & \{\sqrt{\omega(i)\omega(j)}[\omega(i)+\omega(j)]|\omega_\Gamma(k)-\omega(k)|/c(k) \\ & + \text{ similar terms with } i,\ j, \text{and } k \text{ interchanged}\}/3!,\end{aligned} \tag{29}$$

with $\omega_\Gamma(k)$ being the frequency at the Γ point (zone center) for mode k and $c(k)$ is the phonon speed for the branch and momentum labeled by k. A zero (nonzero) reciprocal lattice vector $\boldsymbol{G}$ accounts for a Normal (an Umklapp) process and $\bar{\gamma}$ is a mode-averaged *rescaled* Grünneissen constant. The reasoning behind this generalization is discussed in the Appendix to this paper. We observe that this approach does not make use of two of the three approximations examined in Ref. 37 as it uses complete phonon dispersions rather than Debye-type approximations and accounts for the effects of optical modes in addition to acoustic modes. It does, however, make use of the third approximation (that of the elastic continuum) but we believe that it can provide good qualitative results nonetheless.

III. NUMERICAL AND COMPUTATIONAL DETAILS

A. Electronic parameters for sample under study

Before discussing the electronic transport coefficients S, σ, and $\kappa_{\rm el}$, we first note that the system of the present study, sample 7 of Meddins and Parrott's study,[9] is a sintered $Si_{0.754}Ge_{0.246}$ n-type doped alloy with P impurities acting as donors. In their study, Meddins and Parrott determined the carrier concentration of the sample at room temperature to be 9.4×10^{25} m^{-3} (we take this value to be a reasonable approximation of $N_{\rm don}$) and its density to be around

TABLE I. Parameters for the electronic contributions to ZT derived from comparison with experimental data. We list the name of the parameter, its value, the measured quantity with which it is associated, the corresponding equation for that quantity, and the figures in which the theoretical behavior of that quantity is plotted alongside experimental measurements. A dagger indicates that this quantity was selected rather than directly fitted.

Parameter	Value	Quantity	Equation	Figure
m_e^{dos}	$0.51m_e$	$\lvert S\rvert$	(5) via (3)	3
c_L	7504 ms^{-1} †	σ_{ac}	(13)	4
$\mathcal{C}$	0.0013 †	σ_n	(32)	4
E_D	10.5eV †[11]	σ_{ac}	(13)	4
m_c*	$0.45m_e$ †	σ_{ac}	(13)	4
ν	0.4	σ_n	(32)	4
$m_{\parallel}^*$	$1.10m_e$	...	...	...
$m_{\perp}^*$	$0.35m_e$	...	...	...
G	$3.2\times10^{23}\left(\frac{T}{300}\right)^{2.3}$ m^{-1} V^{-1} s^{-1}	κ	(2) via (18) and (19)	4, 10

2860 kg m^{-3} (this is lower than might be expected through a weighted averaging of the masses of the component elements and could indicate that the sample is somewhat porous). For our calculations, we will also require the relative locations of the conduction band edge E_c, the donor energy level E_d, and the valence band edge E_v. Since Meddin and Parrott did not measure these values in their study, we must estimate them. We set $E_c = 0$ so that it functions as a reference energy, and take our values for the valence band edges from Fig. 8 of Ref. 41 and the donor levels from Table 9.1 on page 269 of Ref. 19. Accordingly, for Si, we take $E_d = 0.045$ eV and $E_v = E_c - 1.170 + [4.73\times10^{-4}/(636+T)]T^2$ eV; and for Ge, we take $E_d = 0.012$ eV and $E_v = E_c - 0.7437 + [4774\times10^{-4}/(235+T)]T^2$ eV. We then estimate the corresponding values for the alloy as a weighted average of the values for Si and Ge. This gives us values of $E_d = -0.037$ eV and a set of temperature dependent values for E_v. We take $N_{\mathrm{val}} = 6$, as the composition of our sample places us within the Si-like region.[35] The value of c_L is taken to be 7504 ms^{-1}, which is the speed of the LA mode at the q point closest to Γ in the Monkhorst Pack grid used in our phonon calculations. Table I lists the electronic parameters used in this work.

B. Technical aspects for calculations of phonon-related quantities

Firstly, we replace Brillouin zone integration of required functions with summation over a set of momenta and associated weighting factors generated through a Monkhorst-Pack (MP) scheme.[42] In order to avoid complication in the numerical calculation of velocities of phonons, we chose to use a shifted set of MP points (i.e., a set that does not include symmetry points in the zone). Secondly, we note that Eq. (28) includes a number of δ-function terms that are difficult to evaluate numerically and must be approximated. We follow the approximations used in Refs. 39 and 40 and replace the exact momentum conservation condition with an approximation as follows:

$$\boldsymbol{q}+\boldsymbol{q}'\pm\boldsymbol{q}''-\boldsymbol{G}=0\rightarrow\lvert q_\mu+q'_\mu\pm q''_\mu-G_\mu\rvert\leqslant\Delta_\mu,\quad \mu=x,y,z, \tag{30}$$

with Δ_μ being the absolute value of the smallest momentum division of the MP grid in the μ direction. This replacement is required as the use of the MP grid entails that the exact condition can never be fulfilled; an approximation is needed in order to obtain nonzero values of the inverse anharmonic relaxation time. Previous calculations[39,40] have shown that this procedure yields reasonable results. We use a set of 26 $\boldsymbol{G}$ vectors, which produces a stable result in this case. Thirdly, we use the definition of the Dirac δ function in terms of a Gaussian function:

$$\delta(y)=\lim_{\sigma\rightarrow0}\frac{1}{\sigma\sqrt{\pi}}e^{-y^2/\sigma^2}, \tag{31}$$

where $0\leqslant y\leqslant 0$, the energy conservation condition has been rescaled by $\omega_{\Gamma\,\mathrm{MAX}}$ (the largest zone-center frequency), and we choose a broadening factor σ that is numerically appropriate (for this study, we use $\sigma = 0.5$). If $\delta(y) < 0.01$ for a given set of modes, we instead set it to zero, in order to avoid spurious contributions arising from large quantities far from the center of the Gaussian. Table II lists the parameters used in the calculations of phonon-related quantities.

C. Calculations of phonon eigensolutions and velocities

As discussed in the previous section, for numerical evaluation of κ_{ph}, we require to calculate phonon frequencies $\{\omega(\boldsymbol{q}s)\}$, eigenvectors $\{\boldsymbol{e}(\boldsymbol{q}s)\}$, and velocities $\{\boldsymbol{v}(\boldsymbol{q}s)\}$. We obtained these quantities through the application of density functional theory and linear response theory [the combination known as density functional perturbation theory (DFPT)],[17,18] as implemented in the routines incorporated into the QUANTUM ESPRESSO package.[43] Norm-conserving pseudopotentials utilizing a local density approximation (LDA) to the DFT[44] were employed in our calculations.

TABLE II. The various parameters determining the behavior of κ_{ph}, their values, and the quantities and equations associated with them.

Parameter	Value	Quantity	Equation
L	0.2 μm	$\tau_{\mathrm{BD}}^{-1}(\boldsymbol{q}s)$	(22)
P	400.0	$\tau_{\mathrm{MD}}^{-1}(\boldsymbol{q}s)$	(23)
A	0.8 eV	$\tau_{\mathrm{EP}}^{-1}(\boldsymbol{q}s)$	(26) via (27)
$\bar{\gamma}$	0.63	$\tau_{\mathrm{AH}}^{-1}(\boldsymbol{q}s)$	(28)

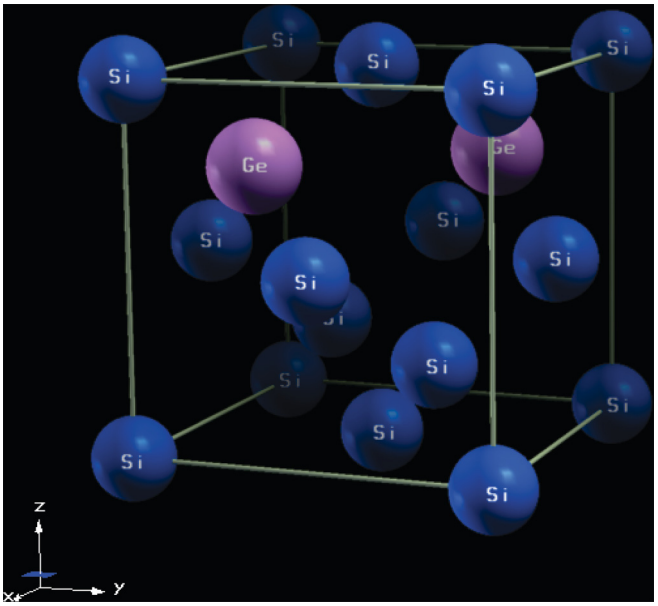

FIG. 1. (Color online) The $Si_{0.75}Ge_{0.25}$ cell used in our DFT calculations. Blue (dark) spheres represent Si atoms, and lilac (light) spheres represent Ge atoms. Image generated using XCRYSDEN (see Ref. 47).

We simulated the $Si_{0.75}Ge_{0.25}$ crystal structure by considering the eight-atom cubic unit cell depicted in Fig. 1. We do not expect there to be any significant error arising from the slight discrepancy in alloy composition, nor from the (inevitably) ordered nature of this alloy model when comparing our results with measurements on the $Si_{0.75}Ge_{0.25}$ disordered alloy studied in Ref. 9. Using a cell dimension of $a = 5.48$ Å consistent with Vegard's law of the weighted average (i.e. $a = 0.75a_{Si} + 0.25a_{Ge}$), we adopted shifted $4 \times 4 \times 4$, $6 \times 6 \times 6$, $8 \times 8 \times 8$, $10 \times 10 \times 10$ Monkhorst-Pack grids with kinetic energy and density cutoffs of 15.0 and 60.0 Ry, respectively, and performed an electronic calculation while allowing the atomic coordinates in the cell to relax. DPFT calculations were carried out using the equivalent unshifted grids, and from the resulting force constants we calculated the phonon eigensolutions for the original shifted grids. From these results, the thermal conductivity matrix was calculated, and κ_{ph} was taken to be the average value of the diagonal components, neglecting the off-diagonal values as artifacts of our model. Comparisons of the thermally averaged mean-free path due to anharmonic scattering for a system with $\bar{\gamma} = 0.5$ at $T = 100$, 600, and 1200 K were made in order to check convergence (see Table III). As can be seen, these results are not very promising, however, if we compare values of κ_{ph} for various grids calculated using the parameters (see Table II) obtained through the fitting procedure used on $10 \times 10 \times 10$ results and listed in Table IV, we see a very different picture. Here, the convergence is monotonic, and is of the order of less than 30% in the worst case ($T = 1200$ K) for the finest grid, which is at the limit of our computational capacity. We suspect that this difference in behavior may be due to divergences in the value of the anharmonic mean-free path that are present at low values of $\boldsymbol{q}$;[38] these may become troublesome as finer grids (containing ever smaller $\boldsymbol{q}$ values) are employed. As Ziman notes in his discussion of the divergence problem in Ref. 38, the cure is the inclusion of additional forms of scattering (usually boundary scattering); since we have (as far as we are aware) accounted for all major sources of scattering in our final calculation of κ_{ph}, this may be the reason for the improvement in convergence. The decrease in convergence as T is increased is likely due to the increasingly important role that the anharmonic scattering plays at higher temperatures; however, we should note that in the region of interest its lack of convergence is still somewhat tamed by the presence of other scattering mechanisms. This also indicates that the mean-free path for anharmonic scattering should not be used alone in order to estimate convergence; the effects of other scattering processes must be taken into account.

There remains only the choice of an appropriate MP grid for our calculation. As implied above, we used the eigensolutions corresponding to the $10 \times 10 \times 10$ grid in our calculation of κ_{ph}; it was felt that this grid presented the best trade-off between convergence and computational effort available.

IV. RESULTS

A. Electronic properties

Figure 2 shows the temperature variation of the Fermi energy E_F for the n-doped sample number 7 in Ref. 9 with temperature. There is clear evidence that the system shows extrinsic-type behavior in the region of interest. We assumed that acoustic scattering was dominant and so fixed the value of the scattering parameter at $s = -0.5$. We then numerically fitted our expression for $|S|$ to the experimental data of Ref. 9 using the algorithms described in (for example) Ref. 45 in order to find an optimal value of m_e^{dos} (displayed in Table I). Since this also required the calculation of E_F, we are able to display the behavior of that (see Fig. 2) and of $|S|$ (see Fig. 3) with temperature.

TABLE III. Convergence of the mean-free path due to anharmonic scattering calculated on successively more fine shifted MP grids for $T = 100$ K and $\bar{\gamma} = 0.5$. Here, $\Delta\lambda_{AH}^{TE}$ is the relative difference between the value of λ_{AH}^{TE} computed for the present grid and the value of λ_{AH}^{TE} computed for its successor, expressed as the nearest whole percentage of the smallest value.

		$T = 100$ K		$T = 600$ K		$T = 1200$ K	
MP Grid	Number of grid points	λ_{AH}^{TE} (m)	$\Delta\lambda_{AH}^{TE}$	λ_{AH}^{TE} (m)	$\Delta\lambda_{AH}^{TE}$	λ_{AH}^{TE} (m)	$\Delta\lambda_{AH}^{TE}$
$4 \times 4 \times 4$	12	0.3445×10^{-7}	...	0.3567×10^{-8}	...	0.1748×10^{-8}	...
$6 \times 6 \times 6$	36	0.6586×10^{-6}	181%	0.5530×10^{-7}	145%	0.2661×10^{-7}	142%
$8 \times 8 \times 8$	80	0.3251×10^{-6}	100%	0.3041×10^{-7}	81%	0.1485×10^{-7}	79%
$10 \times 10 \times 10$	150	0.8427×10^{-6}	159%	0.7355×10^{-7}	141%	0.3560×10^{-7}	139%

TABLE IV. Convergence of κ_{ph} at $T = 100$ K due to anharmonic scattering as MP grids are made successively more fine, using the parameters of Table II. Here, $\Delta\kappa_{\text{ph}}$ is the relative difference between the value of κ_{ph} computed for the present grid and the value of κ_{ph} computed for its successor, expressed as the nearest whole percentage of the smallest value.

	$T = 100$ K		$T = 600$ K		$T = 1200$ K	
MP grid	κ_{ph} (W m^{-1} K^{-1})	$\Delta\kappa_{\text{ph}}$	κ_{ph} (W m^{-1} K^{-1})	$\Delta\kappa_{\text{ph}}$	κ_{ph} (W m^{-1} K^{-1})	$\Delta\kappa_{\text{ph}}$
$4 \times 4 \times 4$	3.4321	...	1.3251	...	0.79718	...
$6 \times 6 \times 6$	4.8023	40%	4.2119	218%	3.8353	381%
$8 \times 8 \times 8$	3.3913	42%	2.8882	45%	2.3016	67%
$10 \times 10 \times 10$	3.3795	0.35%	3.3841	17%	2.9478	28%

Figure 4 shows the temperature variation of σ. As with the Seebeck data, it can be seen from Meddins and Parrott's experimental data[9] that there is no obvious transition to a region of intrinsic-type conductivity for the temperature range of interest. However, in order to properly account for the temperature dependence of σ_n, it was found that multiplication by an *ad hoc* term was necessary:

$$\sigma_n = \sigma_{\text{ac}} \mathcal{C} T^{\nu}, \tag{32}$$

where $\mathcal{C}$ and ν are adjustable parameters. The need for these terms may be a result of inelastic scattering processes that are neglected in our analysis (see Ref. 19); the necessity of including a similar factor has also been noted in a recent theoretical analysis of conductivity data in BiTe-based systems.[46]

We take $E_D^2 m_c^*/\mathcal{C}$ and ν as the overall adjustable parameters for our final fit, obtaining a value of $3286.90 m_e$ eV^2 for the former and 0.4 for the latter. Choosing $E_D = 10.5$ eV, consistent with Ref. 11, $\mathcal{C} = 0.013$ and $m_c^* = 0.45 m_e$, we obtain the following values for the parallel and transverse masses by using the equations relating them to m_c^* and m_e^{dos}:[19] $m_{\parallel}^* = 1.10 m_e$ and $m_{\perp}^* = 0.35 m_e$. It should be observed that $m_{\perp}^*$ is slightly more than twice what one would expect from a linear average of the corresponding Si and Ge masses, whereas $m_{\parallel}^*$ is more or less what is expected; this is because our m_c^* and m_e^{dos} values are larger than expected. We display the resulting parameters in Table I.

There is also a small contribution to σ from σ_h, which can have a large effect on the bipolar contribution to the thermal conductivity. We modelled the hole conductivity using Eq. (19) and obtained the parametrization displayed in Table I through consideration of the total value of the thermal conductivity, as described below. We should note that although Fig. 4 displays the *sum* of the two conductivities, σ_h/σ_n is small enough within the temperature range of the experimental data that the effect of the inclusion of the hole contribution on the curve is negligible (at $T = 1100$ K, σ_h is about 2% of σ_n, and for lower temperatures it is smaller), supporting our decision to ignore it when fitting to the experimental conductivity data. These assumptions do not hold for extremely high temperatures, however, at $T = 1200$ K, σ_h is about 8% of σ_n, and will likely increase; our value for σ here is less trustworthy than for lower temperatures. However, this regime is outside the temperature range for which we possess experimental data.

B. Phonon dispersion curves and density of states

Figures 5 and 6 display the phonon dispersion curves along the Cartesian axes of the system and the density of states for the ordered $Si_{0.75}Ge_{0.25}$ alloy with eight-atom unit cell utilizing a $10 \times 10 \times 10$ MP grid. Results are presented for both the relaxed and unrelaxed cases. We will note a number of general features of interest in the relaxed case. Firstly, the dispersions of phonon branches in the [001] direction differ from those in the [100] and [010] directions, which

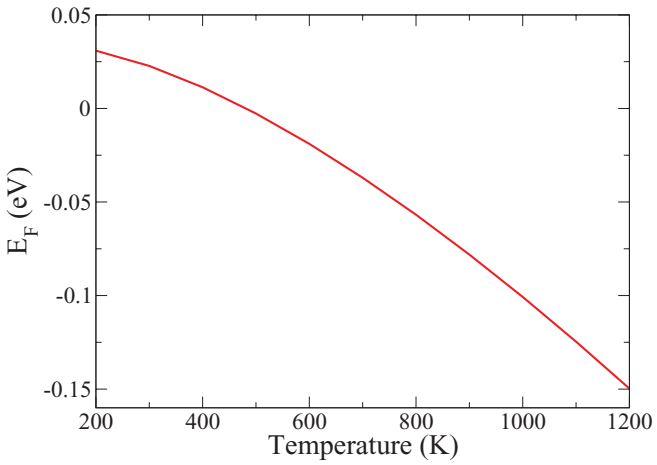

FIG. 2. (Color online) Calculated behavior of E_F with temperature for the system of our study.

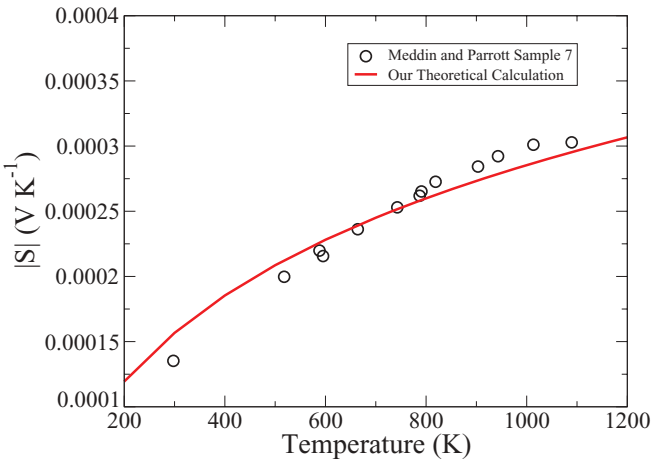

FIG. 3. (Color online) Calculated behavior of $|S|$ compared with experimental data from Fig. 4 of Ref. 9. (Data used with the permission of IOP Publishing Ltd.)

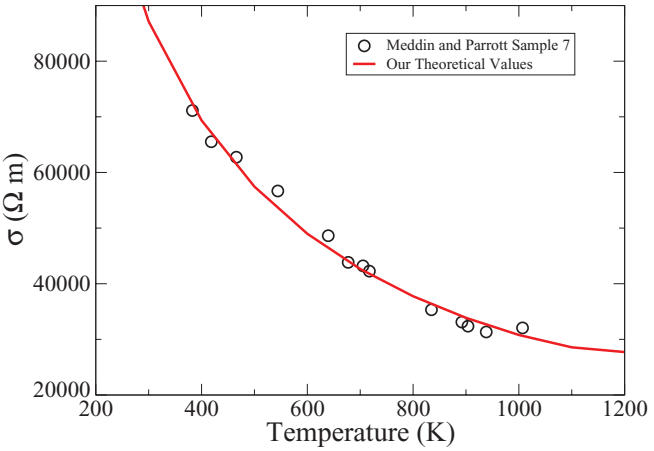

FIG. 4. (Color online) Theoretical behavior of σ compared with experimental data taken from Fig. 3 in Ref. 9. (Data used with the permission of IOP Publishing Ltd.)

are identical (see Fig. 5). This should not be surprising, as if we refer to Fig. 1, we can see that the positioning of the Ge atoms in the cell distinguishes that direction from the others. From the dispersion relations, we can also see that a pair of "gaps" appear in all three directions between frequencies of about 300–350 cm^{-1} and about 400–425 cm^{-1}. By comparison with Fig. 6, we can see that the locations of these gaps roughly correspond to frequencies between approximately 310–345 cm^{-1} and approximately 400–428 cm^{-1} where the phonon density of states has fallen to zero. It is thus clear that two phononic gaps exist for the structure modelled in our work. The presence of such gaps in thin SiGe systems has been noted and discussed previously.[48,49] This is a consequence of our use of an ordered model that resembles a superlattice of unequal period upon repetition of the unit cell in our DFPT calculations; strictly speaking, we should use a larger, cubically symmetric cell in our calculations, but we are limited by our computational resources. In order to overcome this, we assume as a first approximation that any macroscopic system will consist of randomly oriented cells of this kind, and hence that the isotropic lattice thermal conductivity can be considered to be the average of the diagonal components of the thermal conductivity matrix for a single cell. We do not feel that this approximation will lead to significantly different results from calculations carried out using a different choice of cell.

Returning to our discussion of the DFPT results, we may support the notion that the ordering of the alloy is the chief factor in the existence of the phononic gaps by considering the phonon dispersion curves for the modelled SiGe alloy along each of the three Cartesian directions. A comparison between the relaxed and unrelaxed results shown in Fig. 5 indicates that the dispersions of low frequency branches (comprising the acoustic modes and optical modes below around 300 cm^{-1}) are relatively unaffected by bond relaxation (there is some small modification as 300 cm^{-1} is approached, but nothing significant). However, the same cannot be said of the higher-frequency optical branches, whose behavior is considerably modified. Examination of the phonon density of states in Fig. 6 would seem to support this—the unrelaxed and

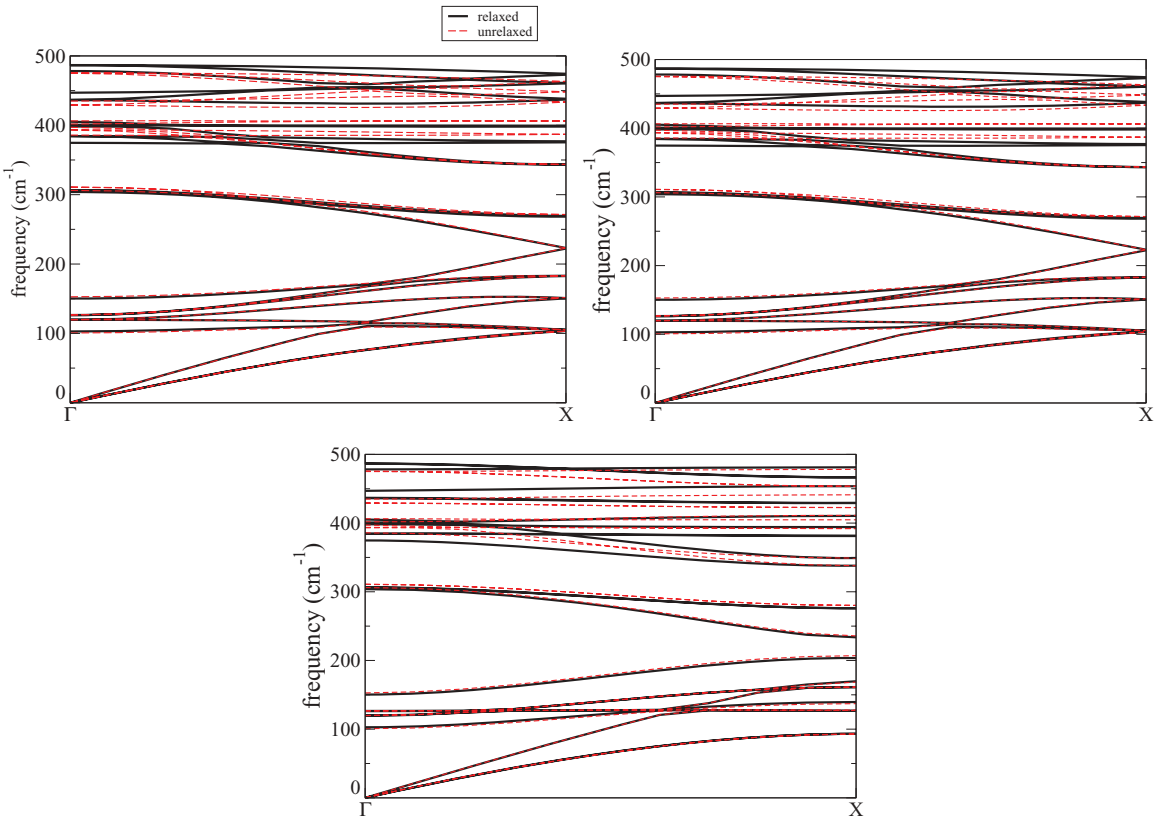

FIG. 5. (Color online) Comparison of phonon dispersion relations along the [100] (top left), [010] (top right), and [001] (bottom center) directions for the ordered $Si_{0.75}Ge_{0.25}$ system discussed in the text.

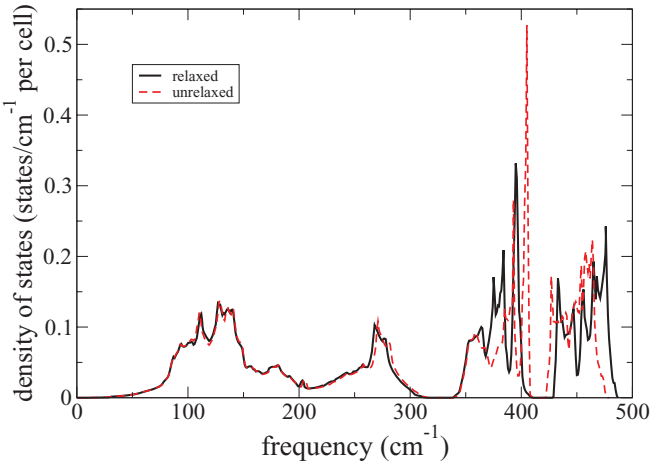

FIG. 6. (Color online) Phonon density of states against frequency for the ordered $Si_{0.75}Ge_{0.25}$ alloy discussed in the text. Note the pair of frequency "gaps" in the vicinity of 325 and 420 cm^{-1}.

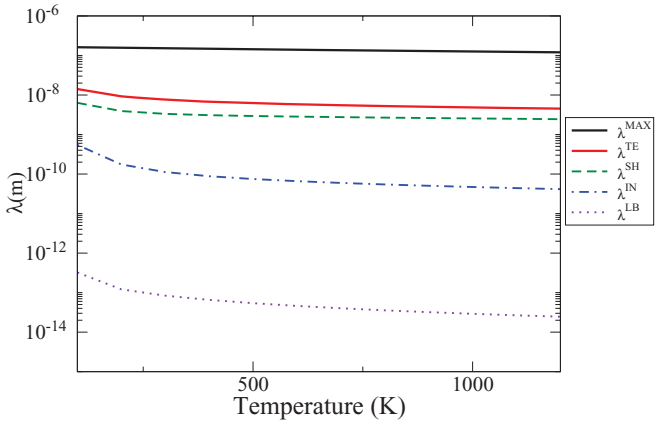

FIG. 7. (Color online) The temperature dependence of the phonon mean-free path (MFP) calculated using various methods, compared with that of the relaxation length of the mode whose weighted contribution to κ_{ph} is the greatest (λ^{MAX}).

the relaxed cases are qualitatively similar (though not identical) below around 350 cm^{-1}, which includes the lower of the two frequency gaps. Above this frequency, we can see that there are considerable differences in the locations of the peaks in either case, and the size of the higher frequency gap is slightly *increased* by bond relaxation from around 410–422 cm^{-1} to around 400–428 cm^{-1}. We can therefore conclude that bond relaxation affects the size of one gap in the system, but that it does not give rise to the gaps themselves.

C. Phonon mean-free path

We now turn to an interesting question that has perhaps not received the consideration that it deserves: the notion of the mode-average phonon mean-free path (MFP) λ. The issue in question is the precise *form* of the mode averaging that one can employ, and it is this which we examine in what follows.

One prescription that has been used in calculations of this quantity (for example, in Ref. 50) is a simple thermal averaging:

$$\lambda^{\mathrm{TE}} = \frac{\sum_{\boldsymbol{q}s} \lambda_{\boldsymbol{q}s} \bar{n}_{\boldsymbol{q}s}}{\sum_{\boldsymbol{q}s} \bar{n}_{\boldsymbol{q}s}}, \tag{33}$$

where $\lambda_{\boldsymbol{q}s} = c_s(\boldsymbol{q})\tau(\boldsymbol{q}s)$. Another suggested prescription (see, for example, Refs. 38 and 39 for theoretical discussions and Ref. 51 for a proposed measurement technique) weights the value of $\lambda_{\boldsymbol{q}s}$ at a given mode and momentum with the corresponding specific heat and velocity:

$$\lambda^{\mathrm{SH}} = \frac{1}{\bar{c}C} \sum_{\boldsymbol{q}s} C_{\boldsymbol{q}s} c_s(q) \lambda_{\boldsymbol{q}s} = \frac{1}{\bar{c}C} \sum_{\boldsymbol{q}s} \kappa_{\mathrm{ph}}(\boldsymbol{q}s), \tag{34}$$

where $\bar{c} = \sum_{\boldsymbol{q}s} c_s(\boldsymbol{q}) \bar{n}_{\boldsymbol{q}s} / \sum_{\boldsymbol{q}s} \bar{n}_{\boldsymbol{q}s}$ is the mode-averaged velocity, $C_{\boldsymbol{q}s} = \omega^2(\boldsymbol{q}s) \bar{n}_{\boldsymbol{q}s}(\bar{n}_{\boldsymbol{q}s} + 1)$ is the specific heat for a given mode, $C = \sum_{\boldsymbol{q}s} C_{\boldsymbol{q}s}$ is the overall specific heat, and $\kappa_{\mathrm{ph}}(\boldsymbol{q}s)$ is the phonon conductivity for a given mode. We tend to prefer this definition as it relates more directly to the measured quantity of interest, which is to say the lattice thermal conductivity.

Furthermore, we may also wish to calculate the MFPs arising from different contributions to scattering; in this case, we replace the total $\tau(\boldsymbol{q}s)$ in a given equation with the $\tau(\boldsymbol{q}s)$ corresponding to the contribution of interest. We will denote the contributions of interest with subscripts as follows: total anharmonic (AH), Normal (N), Umklapp (U), and also compare with the values of the following definition of the MFP:

$$\frac{1}{\lambda^{\mathrm{IN}}} = \frac{\sum_{\boldsymbol{q}s} \tau_{\boldsymbol{q}s}^{-1} c_s^{-1}(\boldsymbol{q}) \bar{n}_{\boldsymbol{q}s}}{\sum_{\boldsymbol{q}s} \bar{n}_{\boldsymbol{q}s}}, \tag{35}$$

and with values of the variationally derived lower bound of the MFP:[38]

$$\frac{1}{\lambda^{\mathrm{LB}}} = \frac{\bar{c}}{C} \sum_{\boldsymbol{q}s} \frac{C_{\boldsymbol{q}s} \tau^{-1}(\boldsymbol{q}s)}{c_s^2(\boldsymbol{q})}. \tag{36}$$

In Fig. 7, we plot the mean-free paths (MFPs) calculated using all these methods and utilising all available phonon modes. We also display λ^{MAX}, which is the MFP associated with the mode whose weighted contribution to κ_{ph} is the greatest. We can see that there is a large and obvious difference between the results of the various methods, with λ^{TE} and λ^{SH} being the most similar, λ^{IN} being an order of magnitude smaller than the latter. λ^{LB} is smaller still; this is unsurprising since it is the lower bound of the MFP. λ^{MAX} is larger than all of these, consistent with the analysis of Ref. 52, which notes that mode-averaged MFPs are likely to greatly underestimate the degree to which modes with long MFPs contribute to κ_{ph} in systems where the effects of defect scattering are strong (as is in fact the case in this alloy—see the next section for more details). Because of this, one can immediately rule out λ^{LB} and λ^{IN} as good definitions of the MFP; they are far too small. With regards to λ^{SH}, as we see here and in Richardson *et al.*,[52] it also underestimates the contribution from long MFP modes. We find that λ^{TE} also offends in this regard (though not quite as badly as λ^{SH}). This entails that one must exercise caution when interpreting MFP data—not only can it be misleading in certain systems, but its value is strongly dependent on the method by which it is calculated; in the case of the present system, even

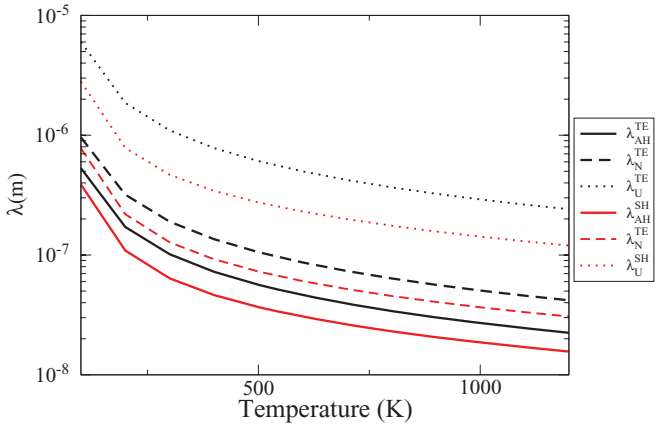

FIG. 8. (Color online) The temperature dependence of the phonon mean-free path (MFP) due to total anharmonic scattering, Umklapp and Normal processes as calculated by thermal averaging (TE) and from the thermal conductivity (SH).

if λ^{SH} and λ^{LB} did not likely underestimate the value of the MFP, they do not give the same answer as to its value. We do not know of any strong theoretical reason for preferring one definition over the other; however, in a practical sense (as far as thermal conductivity measurements are concerned) we are inclined to prefer λ^{SH}, for its calculation utilises experimental quantities that are readily measured, as in Ref. 51. What is most important, however, is that whichever method one uses is clearly stated.

Figures 8 and 9 display the MFP due to total anharmonic, Normal, and Umklapp scattering for the above mode-averaging schemes. For all cases, we see that the MFP due to Normal processes is typically larger than that of the MFP due to Umklapp processes, suggesting that the latter are generally more important to the overall scattering. We should caution against taking these results as final and definitive, due to the badly convergent nature of the anharmonic MFP discussed in the previous section. However, we think they are likely to be qualitatively reliable.

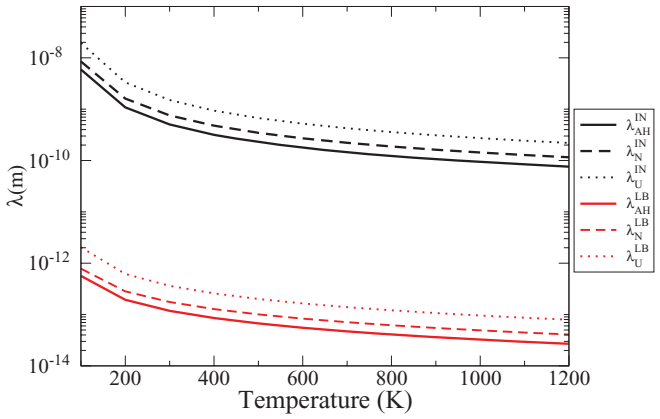

FIG. 9. (Color online) The temperature dependence of the phonon mean-free path (MFP) due to total anharmonic scattering, Umklapp and Normal processes as calculated by thermal averaging of λ_{qs}^{-1} (IN) and from the variational lower bound formula (LB).

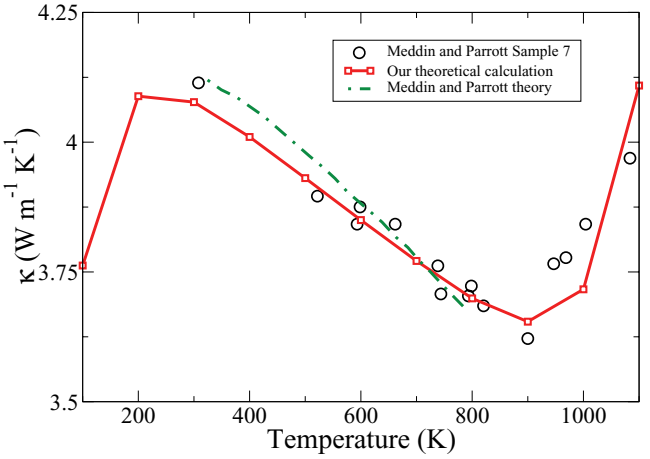

FIG. 10. (Color online) Comparison of the presently calculated values of the thermal conductivity (κ) with the theoretical and experimental values read from Fig. 6(g) in Ref. 9. (Data used with the permission of IOP Publishing Ltd.)

D. Thermal conductivity

Due to the complexity involved in the implementation of the calculation of κ, numerical fitting proved unfeasible, and it was necessary to manually tune the semiadjustable parameters so as to attain results that displayed reasonable agreement with Meddins and Parrott's[9] measurements of the total thermal conductivity κ. The parameters listed in Table II (and used in Fig. 10) and those concerning σ_p in Table I were obtained by choosing a given parameter set, calculating κ_{ph} from the eigensolutions generated for a $10 \times 10 \times 10$ MP grid, adding the results to the κ_{el} values to obtain κ, and then comparing this with the experimental results, and repeating the process with adjusted values of the parameters until good agreement was reached.

Figure 10 displays the resulting values of κ alongside the experimental results of and a theoretical calculation from Ref. 9. Qualitatively speaking, it can be seen that our calculation is a better match to the data than theirs for the region in which they give theoretical values aside from the data point at the lowest temperature, which is somewhat undershot, and that our calculation has a wider range of validity. For temperatures greater than 900 K, where the bipolar contribution is dominant (and thus the behavior is determined by our parametrization of σ_p), the curve matches the data less well; in fact, the form of the data is such that it made selecting appropriate values for the behaviour of G difficult, which should be kept in mind when considering the accuracy of our calculation in this region. It should be kept in mind that the value of the material density ρ used for the calculation of κ_{ph} is the weighted average value of 3077.5 kg m^{-3} rather than the measured value of 2860 kg m^{-3} found in Ref. 9; but any errors resulting from this difference will be absorbed into the values of A and $\bar{\gamma}$, which control the strength of the scattering processes that exhibit density dependence.

Examining the results displayed in Table II, we note that our fit was obtained using a value of L, which is the lower limit of that expected by Ref. 9, suggesting a fairly small crystallite size. P is fairly large, indicating that we are accounting for scattering from a large number of defects consistent with our discussion of the mean-free path results; it would not be

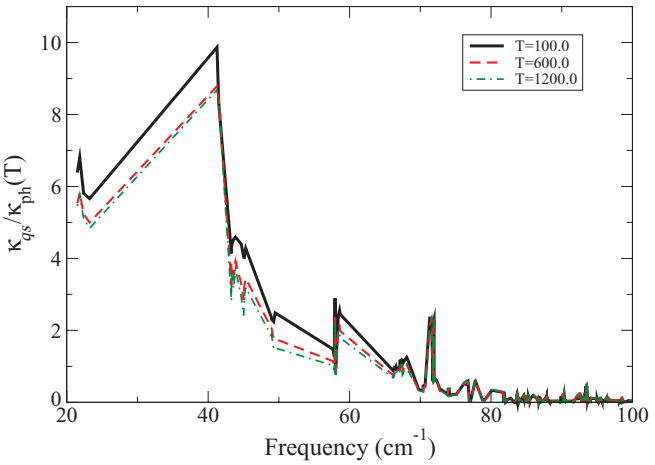

FIG. 11. (Color online) Frequency dependence of $\kappa_{qs}(T)$ normalised by $\kappa_{ph}(T)$ in our calculation. While κ_{qs} is the contribution without the weight factor associated with $\boldsymbol{q}$, the total contribution κ_{ph} is computed after summing κ_{qs} with the required weight factor associated with $\boldsymbol{q}$.

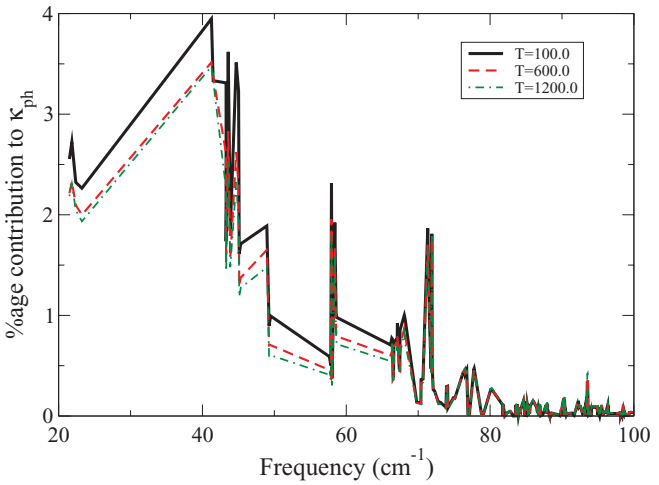

FIG. 12. (Color online) Percentage contribution of each frequency to $\kappa_{ph}(T)$. Note that this includes the weighting arising from our use of MP summation.

surprising if the large concentration of impurities in the heavily doped sample were to play a role in this. As a result of the lack of experimental data in the regime where electron-phonon scattering has an important effect, the value of A cannot be considered to be precise, however, a finite but not too large value seems to be required in order to properly capture the behavior of the system in the lower-temperature region. Due to the number of adjustable parameters and the method we have had to adopt in order to tune them, we cannot properly say that this is a *uniquely* optimal set, but it is certainly a good one, and it seems plausible that any other parameter set that gives a good fit will be reasonably similar.

We also should note that we obtain better agreement with experiment at temperatures in the 700–900 K than Garg *et al.* attain for their computation of κ for undoped $Si_{0.3}Ge_{0.7}$ [presented in Fig. 3(a) of Ref. 15]; this should not be wholly surprising since we are making use of a semiempirical approach; this improved agreement may be as much due to our use of adjustable parameters as it is to the inherent virtues of our approach.

We now turn to the frequency dependence of κ_{ph}, presented in Fig. 11 for three temperatures with frequencies below 100 cm^{-1} ($\approx$3 THz) corresponding to points in momentum space coinciding with a $14 \times 14 \times 14$ MP grid. The dominant frequencies are all contained within this area, which is consistent with the results presented in Fig. 2(a) in the paper by Garg *et al.*[15] for $Si_{0.5}Ge_{0.5}$ alloys calculated using the virtual crystal approximation, and the "double peak" structure of the two most dominant modes is reproduced, although the peaks are situated at higher frequencies in our case. From Fig. 5, we can see that this frequency range is occupied by acoustic modes, entailing that they contribute the most to κ_{ph}. However, there are some differences. One of these is that in our case the magnitude of the normalized values does not appear to be as strongly affected by increases in temperature, and there is a pronounced "spike" in the contribution from a frequency near 70 cm^{-1}. Another is that our values appear to be larger by a factor of around 6.25. These differences may both be a function of methodology and of the differing compositions of our materials.

However, one must be careful when drawing conclusions from these data as to the relative contributions of various frequencies to κ_{ph}. This is because in our actual calculations, we make use of the MP momentum summation scheme, and therefore each frequency displayed in Fig. 11 in fact makes a contribution to κ_{ph} that is *weighted* according to the $\boldsymbol{q}$ point with which it coincides. We display the percentage contribution to κ_{ph} of each frequency following such weighting in Fig. 12. It is apparent that the general behavior with temperature is consistent with that of Fig. 11. However, we can also see that the weighting of the contributions has drastically altered our conception of how low frequencies contribute to κ_{ph}, for while the overall trend in the degree of contribution is still downwards for frequencies greater than 40 cm^{-1}, the contributions of a small number are strongly enhanced. For example, the contributions of two frequencies in the region of 45 cm^{-1} are far greater than would be expected from Fig. 12, in fact contributing more than the subdominant frequency of that figure.

There is a caveat with regards to these data, however. We have naively plotted the frequency data without regard for degeneracy or the manner in which numerical error separates out what should be degenerate modes, entailing that we may be undercounting the contribution of some frequencies (for example, those corresponding to transverse acoustic modes). But it would seem likely that this would not overly affect our general conclusion, which is that when accounting for the contributions of various modes to κ_{ph} one should take into account the degree to which each mode is weighted by the MP summation scheme, as it is entirely possible that not doing so might mislead as to which modes are in fact dominant, and to what degree.

E. Figure of merit

Having calculated the relevant electronic and vibrational contributions, we are now in a position to calculate the figure of merit ZT for Sample 7 in Ref. 9. In Fig. 13, we compare our

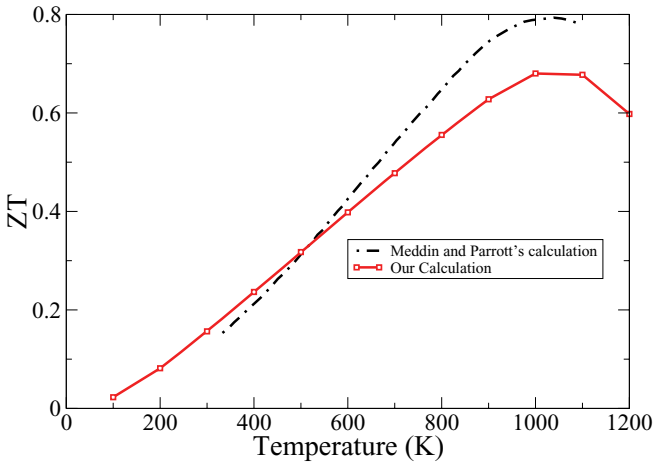

FIG. 13. (Color online) Comparison of the calculation of ZT in the present study with that of Fig. 9 in Ref. 9. (Data used with the permission of IOP Publishing Ltd.)

results with the calculation performed by Meddins and Parrott, which is based on their theoretical model detailed in Ref. 9.

There is reasonable qualitative agreement between our results and the results presented by Meddins and Parrott.[9] However, in quantitative terms, there is a discrepancy of around 16% at 1000 K, and at lower temperatures, our results are slightly larger than theirs. One factor that may account for much of this difference is that Meddins and Parrott do not appear to include the bipolar contribution to κ_{el} in their analysis, and since it is at high temperatures that that contribution is dominant, it is unsurprising that their values of ZT are greater than ours in this region. From our numerical results, we suggest that for the modelled $Si_{0.75}Ge_{0.25}$ alloy values of $ZT > 0.5$ can be expected throughout the high-temperature range of around 750–1200 K, with a maximum of approximately 0.68 at around 1000 K.

A comparison with, and comment on, the work carried out by Minnich *et al.*,[11] is also appropriate. These authors applied a detailed model, similar to that adopted by Vining,[10] of the electronic behavior and of the phonon contribution to κ_{ph} to experimental results for n-doped $Si_{0.8}Ge_{0.2}$ (where N_{don} was obtained by fitting to experimental results) and for n- and p-doped $Si_{0.7}Ge_{0.3}$ where a number of samples with different N_{don} were available. The results for the n-doped $Si_{0.7}Ge_{0.3}$ sample with $N_{don} = 7.3 \times 10^{25}$ m^{-3} are the most relevant here, since the composition and N_{don} of this sample are reasonably close to that of the sample treated in this study. In the fourth panel of Fig. 1 in Ref. 11, they display ZT for their n-type $Si_{0.7}Ge_{0.3}$ samples, and for the sample of interest, it can be seen that the results are qualitatively similar up to around $T = 1000$ K, with a peak at a slightly larger value of ZT (closer to the 0.8 of Meddins and Parrot's results[9] than the 0.7 of ours) and a far sharper decrease than we observe at higher temperatures. Some of this difference is likely to arise from our different approaches, and some of it from the differences in composition between our samples. However, the qualitative similarities are a good sign.

Our calculation of ZT in an SiGe alloy includes as complete as possible an account of the phonon scattering rates and the effects of the bipolar contribution to thermal conductivity. It is hoped that it will provided a benchmark for future theoretical explorations of the thermoelectric efficiency of more complex systems such as nanowires or superlattices.

V. SUMMARY AND CONCLUSION

In this study, we have examined the theoretical behavior of the thermoelectric figure of merit ZT and its constituent quantities for the case of a sintered $Si_{0.754}Ge_{0.246}$ doped with P impurities examined by Meddins and Parrott.[9] We have established phenomenological models to account for the behavior of the electronic quantities, and have focused in detail on the mechanisms underlying the phonon contribution to the thermal conductivity κ. In this respect, we have developed a full-scale theory of the lattice thermal conductivity considering the role of acoustic as well as optical phonons in Normal and Umklapp three-phonon interactions and included the bipolar contribution to thermal conductivity.

We have made use of density functional methods in order to obtain the required phonon eigensolutions and a detailed calculation of the anharmonic contribution to phonon scattering based on a semiempirical model for anharmonic crystal potential. The subsequent calculation of $\kappa_{ph} + \kappa_e$ shows good agreement with measurements in the entire temperature range 300–1100 K. We have also examined the frequency dependence of κ_{ph}, finding that it is consistent with the previously reported results of Ref. 15 apart from some differences in temperature dependence and have discussed some issues concerning the notion of a mean-free path.

From this information, we have calculated the dimensionless figure of merit ZT and compared it with the (incomplete) calculation in Ref. 9. While, in general, the qualitative behavior of the ZT versus T curve in our work is quite similar to that in Ref. 9, with the more complete theoretical treatment we have predicted values of greater than 0.5 in the temperature range of around 750 to at least 1200 K with a maximum of approximately 0.68 at around 1000 K.

In addition to the study of the thermoelectric properties, we have also examined a more conceptual issue: that of the calculation of the phonon mean-free path. We have shown that in the literature, there exist different prescriptions for evaluation of phonon mean free path, yielding different results. We suggest that care must be exercised in comparing results obtained from different methods of mode averaging procedures.

ACKNOWLEDGMENTS

This work has been carried out with help of the EPSRC (UK) grant No. EP/H046690/1, and Iowerth O. Thomas is grateful for the financial support. The calculations were performed using the Intel Nehalem (i7) cluster (ceres) at the University of Exeter.

APPENDIX: THE ANHARMONIC INTERACTION TERM

While the anharmonic crystal potential involving acoustic phonons has been widely discussed, the contributions due to optical modes have not been fully considered, although Klemens[53] and Ridley and Gupta[54] have given simple presentations of the effects of scattering to and from optical modes.

In this work, we have expressed the anharmonic phonon relaxation time due to three-phonon Normal and Umklapp processes involving acoustic and optical phonon modes, using Eqs. (28) and (29). This form of the anharmonic phonon-phonon interaction was proposed by S. P. Hepplestone[55] and was indeed employed in previously published works,[40,49] but has not yet appeared in print. In this appendix, we shall attempt to justify and present the relevant expression for the cubic anharmocity in crystal potential.

We shall begin with following expression for the third-order perturbative term in the elastic continuum potential, taken from Ref. 26:

$$\mathcal{V}_3 = \sqrt{\frac{\hbar^3}{8\rho^3 V}} \sum_{\substack{\boldsymbol{q}s,\,\boldsymbol{q}'s',\\ \boldsymbol{q}''s''}} \mathcal{T}^{ss's''}_{\boldsymbol{q}\boldsymbol{q}'\boldsymbol{q}''}(a^\dagger_{\boldsymbol{q}s} - a_{-\boldsymbol{q}s})(a^\dagger_{-\boldsymbol{q}'s'} - a_{\boldsymbol{q}'s'}) \times (a^\dagger_{\boldsymbol{q}''s''} - a_{-\boldsymbol{q}'s'})\delta_{\boldsymbol{q}+\boldsymbol{q}'+\boldsymbol{q}'',\boldsymbol{G}}, \tag{A1}$$

where

$$\mathcal{T}^{ss's''}_{\boldsymbol{q}\boldsymbol{q}'\boldsymbol{q}''} = \frac{1}{3!}\sqrt{\frac{qq'q''}{c_s c_{s'} c_{s''}}} A^{ss's''}_{\boldsymbol{q}\boldsymbol{q}'\boldsymbol{q}''}, \tag{A2}$$

with $a^\dagger_{\boldsymbol{q}s}$ ($a_{\boldsymbol{q}s}$) being the phonon creation (annihilation) operator for a given mode $\boldsymbol{q}s$, q being the magnitude of the momentum, and c_s being the speed of a phonon belonging to branch s. Note that c_s is not dependent on $\mathbf{q}$ at this point; this expression is derived on the assumption that we are treating acoustic phonons in the continuum, $\boldsymbol{q} \to 0$, limit, and so we can relate frequency and momentum through the dispersion relation $\omega(\boldsymbol{q}s) \approx c_s q$. Our aim is to reverse-engineer from (A1) a starting point similar to that used by Klemens[56] from which we may derive an expression for the anharmonic term that includes aspects of the behavior of optical phonons while remaining true to the spirit of the original continuum, acoustic approach.

Taking the expression for the angularly averaged modulus of $A^{ss's''}_{\boldsymbol{q}\boldsymbol{q}'\boldsymbol{q}''}$ as a guide:[26]

$$\overline{\left|A^{ss's''}_{\boldsymbol{q}\boldsymbol{q}'\boldsymbol{q}''}\right|^2} = \frac{4\rho^2}{\bar{c}^2}\gamma^2 c_s^2 c_{s'}^2 c_{s''}^2, \tag{A3}$$

we put $A^{ss's''}_{\boldsymbol{q}\boldsymbol{q}'\boldsymbol{q}''} = (2\rho/\bar{c})\gamma c_s c_{s'} c_{s''}$, with $\bar{c}$ being an average phonon speed and γ being the modulus of the Grüneissen constant, and so arrive (following a little algebra, and assuming acoustic dispersions at $q \to 0$) at the expression

$$\mathcal{T}^{ss's''}_{\boldsymbol{q}\boldsymbol{q}'\boldsymbol{q}''} = \frac{2\rho\gamma}{\sqrt{\omega(\boldsymbol{q}s)\omega(\boldsymbol{q}'s')\omega(\boldsymbol{q}''s'')}} B^{ss's''}_{\boldsymbol{q}\boldsymbol{q}'\boldsymbol{q}''}, \tag{A4}$$

$$B^{ss's''}_{\boldsymbol{q}\boldsymbol{q}'\boldsymbol{q}''} = \frac{1}{3!}\frac{\omega(\boldsymbol{q}s)\omega(\boldsymbol{q}'s')\omega(\boldsymbol{q}''s'')}{\bar{c}}. \tag{A5}$$

Equation (A5) has the same general form as the approximation used by Klemens.[56] Indeed, if we replace $\bar{c}$ with the speed $c_{s''}$, then in the limit of small q and assuming an acoustic dispersion, we obtain

$$B^{ss's''}_{\boldsymbol{q}\boldsymbol{q}'\boldsymbol{q}''} = \frac{1}{3!}\omega(\boldsymbol{q}s)\omega(\boldsymbol{q}'s')q'', \tag{A6}$$

which is very similar to the expression Klemens[56] has derived in order to motivate his approximation. We shall use this as the basis for our derivation of the general anharmonic term with which to treat three-phonon interaction involving both acoustic and optical modes.

1. Treatment when $q''s''$ is an optical mode

We shall begin with the situation when $\boldsymbol{q}''s''$ is an optical mode and consider three-phonon processes of the types $ac + ac \rightleftharpoons op$ and $ac + op \rightleftharpoons op$. For small values of q'', we express $\omega_o^2(\boldsymbol{q}''s'') = \omega_{\Gamma o}^2(s'')^2 - c_{s''o}q''^2$. Rearranging this, we may write

$$q'' = \frac{(\omega_{\Gamma o}(s) + \omega_o(\boldsymbol{q}''s''))^{1/2}|\omega_{\Gamma o}(s) - \omega_o(\boldsymbol{q}''s'')|^{1/2}}{c_{so}} \approx \frac{\sqrt{2\omega_o(\boldsymbol{q}''s'')}|\omega_{\Gamma o}(s'') - \omega_o(\boldsymbol{q}''s'')|^{1/2}}{c_{so}}, \text{ as } q \to 0. \tag{A7}$$

Next, we observe that $B^{ss's''}_{\boldsymbol{q}\boldsymbol{q}'\boldsymbol{q}''}$ is identical under exchange of the modes $\boldsymbol{q}s$ and $\boldsymbol{q}'s'$; we account for this in Eq. (A1) by simply multiplying $B^{ss's''}_{\boldsymbol{q}\boldsymbol{q}'\boldsymbol{q}''}$ by a factor of 2 and ignoring subsequent terms where those modes are exchanged. Replacing q'' in $B^{ss's''}_{\boldsymbol{q}\boldsymbol{q}'\boldsymbol{q}''}$ with this expression, we obtain

$$B^{ss's''}_{\boldsymbol{q}\boldsymbol{q}'\boldsymbol{q}''} = \frac{1}{3}\frac{\omega(\boldsymbol{q}s)\omega(\boldsymbol{q}'s')\sqrt{2\omega_o(\boldsymbol{q}''s'')}|\omega_{\Gamma o}(s) - \omega_o(\boldsymbol{q}''s'')|^{1/2}}{c_{s''o}}. \tag{A8}$$

Instead of following Klemens[53] or Ridley and Gupta[54] and assuming that the dominant decay is of the form $\omega_o(\boldsymbol{q}''s'') \approx \omega(\boldsymbol{q}s)/2 \approx \omega(\boldsymbol{q}'s')/2$, we shall be more general; examining the energy conservation condition

$$\omega_o(\boldsymbol{q}''s'') = \omega(\boldsymbol{q}s) + \omega(\boldsymbol{q}'s'), \tag{A9}$$

we may see that

$$\omega(\boldsymbol{q}s) = B\omega_o(\boldsymbol{q}''s''), \tag{A10}$$

$$\omega(\boldsymbol{q}'s') = (1 - B)\omega_o(\boldsymbol{q}''s''), \tag{A11}$$

where we consider values of B between zero and unity. From Eq. (A9), we may write $\sqrt{2\omega_o(\boldsymbol{q}''s'')} = \sqrt{2}[\omega(\boldsymbol{q}s) + \omega(\boldsymbol{q}'s')]^{1/2}$ and so $\omega(\boldsymbol{q}s) = \sqrt{B\omega(\boldsymbol{q}s)}[\omega(\boldsymbol{q}s) + \omega(\boldsymbol{q}'s')]^{1/2}$, and hence

$$B^{ss's''}_{\boldsymbol{q}\boldsymbol{q}'\boldsymbol{q}''} = \frac{1}{3}\frac{\sqrt{2B\omega(\boldsymbol{q}s)}\omega(\boldsymbol{q}'s')[\omega(\boldsymbol{q}s) + \omega(\boldsymbol{q}'s')]|\omega_{\Gamma o}(s) - \omega_o(\boldsymbol{q}''s'')|^{1/2}}{c_{s''o}}. \tag{A12}$$

We may also write

$$\frac{\omega(\boldsymbol{q}'s')}{(1 - B)} \approx \frac{\omega_o(\boldsymbol{q}''s'')|\omega_{\Gamma o}(s) - \omega_o(\boldsymbol{q}''s'')|}{|\omega_{\Gamma o}(s) - \omega_o(\boldsymbol{q}''s'')|} = A^2|\omega_{\Gamma o}(s) - \omega_o(\boldsymbol{q}''s'')|, \tag{A13}$$

where A is defined above, and so acquire

$$B^{ss's''}_{\boldsymbol{q}\boldsymbol{q}'\boldsymbol{q}''} = \frac{A}{3}\frac{\sqrt{B(1-B)\omega(\boldsymbol{q}s)\omega(\boldsymbol{q}'s')}[\omega(\boldsymbol{q}s)+\omega(\boldsymbol{q}'s')]|\omega_{\Gamma o}(s)-\omega_o(\boldsymbol{q}''s'')|}{c_{s''o}}, \tag{A14}$$

from which we may obtain

$$\mathcal{T}^{ss's''}_{\boldsymbol{q}\boldsymbol{q}'\boldsymbol{q}''} = \frac{2\rho\Gamma_o}{\sqrt{\omega(\boldsymbol{q}s)\omega(\boldsymbol{q}'s')\omega_o(\boldsymbol{q}''s'')}}\frac{1}{3!}\frac{\sqrt{\omega(\boldsymbol{q}s)\omega(\boldsymbol{q}'s')}[\omega(\boldsymbol{q}s)+\omega(\boldsymbol{q}'s')]|\omega_{\Gamma o}(s)-\omega_o(\boldsymbol{q}''s'')|}{c_{s''o}}, \tag{A15}$$

where $\Gamma_o = 2A\gamma\sqrt{2B(1-B)}$. It should be noted that in order for Γ_o to have a meaningful value at $q=0$, we require that $\gamma\sqrt{B(1-B)} \propto |\omega_{\Gamma o}(s)-\omega_o(\boldsymbol{q}''s'')|^\alpha$ as $q\to 0$, where $\alpha \geqslant 1/2$, in order to cancel the zero-tending term in the denominator of A. This is a strong constraint on the behavior of γ; however, it is an artifact of the form of the term that we must adopt for numerical simplicity. One could consider using other forms, but then one would have to make use of a frequency window in order to distinguish optical and acoustic terms, a process that is cumbersome and which could introduce its own inaccuracies. In this case, we much prefer to choose the form given above, which is easy to implement numerically.

2. Treatment when $q''s''$ is an acoustic mode

To deal with three-phonon processes of the type $ac + ac \rightleftharpoons ac$, with q'' corresponding to an acoustic mode, we first observe that from the acoustic dispersion relation in the limit of small q, we may derive $q = |\omega_{\Gamma a}(s)-\omega_a(\boldsymbol{q}s)|/c_{sa}$, since $\omega_{\Gamma a}(s) = 0$. From Eqs. (A10) and (A11) and energy conservation, we may obtain $\sqrt{\omega(\boldsymbol{q}s)\omega(\boldsymbol{q}'s')} = \sqrt{B(1-B)}[\omega(\boldsymbol{q}s)+\omega(\boldsymbol{q}'s')]$. These may be used to derive

$$\mathcal{T}^{ss's''}_{\boldsymbol{q}\boldsymbol{q}'\boldsymbol{q}''} = \frac{2\rho\Gamma_a}{\sqrt{\omega(\boldsymbol{q}s)\omega(\boldsymbol{q}'s')\omega_a(\boldsymbol{q}''s'')}}\frac{1}{3!}\frac{\sqrt{\omega(\boldsymbol{q}s)\omega(\boldsymbol{q}'s')}[\omega(\boldsymbol{q}s)+\omega(\boldsymbol{q}'s')]|\omega_{\Gamma a}(s)-\omega_a(\boldsymbol{q}''s'')|}{c_{s''a}}, \tag{A16}$$

where $\Gamma_a = 2\gamma\sqrt{B(1-B)}$. This expression for $\mathcal{T}$ is essentially the same as in Ref. 26. (Note that the value of B here is not necessarily identical to that of B in the previous section when q'' was an optical mode, nor is it necessarily identical with values of B considered for scattering between a different triad of phonon modes.)

3. Form for numerical calculations

For ease of calculation, we take $\Gamma_a = \Gamma_o = \bar{\gamma}$, by analogy with the use of the mode-averaged Grüneissen constant in typical computations of this form. Since contributions from both acoustic and optical q'' now share an identical form, we may suppress the indices which distinguish them and write an overall term:

$$\mathcal{V}_3 = \bar{\gamma}\sqrt{\frac{\hbar^3}{2\rho V}}\sum_{\substack{\boldsymbol{q}s,\,\boldsymbol{q}'s',\\ \boldsymbol{q}''s''}}\frac{\mathcal{B}_{\boldsymbol{q}s,\,\boldsymbol{q}'s',\,\boldsymbol{q}''s''}}{\sqrt{\omega(\boldsymbol{q}s)\omega(\boldsymbol{q}'s')\omega(\boldsymbol{q}''s'')}}\delta_{\boldsymbol{q}+\boldsymbol{q}'+\boldsymbol{q}'',\,\boldsymbol{G}} \times(a^\dagger_{\boldsymbol{q}s}-a_{-\boldsymbol{q}s})(a^\dagger_{-\boldsymbol{q}'s'}-a_{\boldsymbol{q}'s'})(a^\dagger_{\boldsymbol{q}''s''}-a_{-\boldsymbol{q}'s'}), \tag{A17}$$

with

$$\mathcal{B}_{i,j,k} = \{\sqrt{\omega(i)\omega(j)}[\omega(i)+\omega(j)]|\omega_\Gamma(k)-\omega(k)|/c(k) + \text{ similar terms with } i,\ j,\ \text{and } k \text{ interchanged}\}/3!, \tag{A18}$$

where i, j, k label phonon modes, and $c(k)$ is now the *momentum dependent*, i.e., phase speed for the mode k; here, we make a generalization to the case where q no longer tends to zero. From this, we may obtain the expression for the anharmonic single-mode relaxation time used in our calculations—that is, Eq. (28).

We should remark that the assumptions made in deriving the above expression are perhaps somewhat crude: unlike Klemens[53] or Ridley and Gupta,[54] we have not properly considered distinctions in behavior arising from the different ways in which the displacement of optical and acoustic vibrations deform the crystal. However, given that Klemens's expression[53] is equivalent to that of Ridley and Gupta (as the latter have observed[54]), and that the former's derivation shows that the differences amount to a rescaling of the optical Grüneissen constant away from the value it would have were it derived assuming acoustic behavior, we should not be too worried; such a distinction would be ignored by our use of a mode-averaged form of the rescaled Grüneissen constant regardless of the final form of our expression. Indeed, given that all such expressions are strictly valid only in the continuum limit, and that our calculation by necessity extrapolates beyond that limit, we should not expect our expression to be any *worse* an approximation than the others, and in terms of simplicity of numerical implementation and avoidance of problems arising from ambiguities in the labeling of the phonon eigensolutions in the output of *ab initio* codes, we feel that it has much to recommend itself.

[1] A. F. Ioffe, *Semiconductor Thermoelements and Thermoelectric Cooling* (Infosearch Ltd., London, 1957).

[2] R. R. Heikes and R. W. Ure, *Thermoelectricity* (Interscience, New York, London, 1961).

[3] D. M. Rowe, *Thermoelectrics Handbook* (Taylor and Francis Group, London, 2006).

[4] H. J. Goldsmit, *Introduction to Thermoelectricity* (Springer-Verlag, Berlin, 2010).

[5] G. Chen, M. S. Dresselhaus, G. Dresselhaus, J.-P. Fleurial, and T. Caillat, Int. Metall. Rev. **48**, 45 (2003).

[6] Y. Lan, A. J. Minnich, G. Chen, and Z. Ren, Adv. Funct. Mater. **20**, 357 (2010).

[7] B. Poudel, Q. Hao, Y. Ma, Y. Lan, A. Minnich, B. Yu, X. Yan, D. Wang, A. Muto, D. Vashaee, X. Chen, J. Liu, M. S. Dresselhaus, G. Chen, and Z. Ren, Science **320**, 634 (2008).

[8] L. D. Hicks and M. S. Dresselhaus, Phys. Rev. B **47**, 12727 (1993).

[9] H. R. Meddins and J. E. Parrott, J. Phys. C: Solid State Phys. **9**, 1263 (1976).

[10] C. B. Vining, J. Appl. Phys. **69**, 331 (1991).

[11] A. J. Minnich, H. Lee, X. W. Wang, G. Joshi, M. S. Dresselhaus, Z. F. Ren, G. Chen, and D. Vashaee, Phys. Rev. B **80**, 155327 (2009).

[12] G. A. Slack and M. A. Hussein, J. App. Phys **70**, 2694 (1991).

[13] A very preliminary version of our findings was presented at the Fall 2011 Meeting of the Materials Research Society and published in I. O. Thomas and G. P. Srivastava, MRS Proceedings **1404**, mrsf11-1404-w04-03, doi:10.1557/opl.2012.328. However, we should note that many of the results presented therein have been considerably refined and corrected in the present work.

[14] D. A. Broido, M. Malomy, G. Bimer, N. Mingo, and D. A. Stewart, Appl. Phys. Lett. **91**, 231922 (2007).

[15] J. Garg, N. Bonini, B. Kozinsky, and N. Marzari, Phys. Rev. Lett. **106**, 045901 (2011).

[16] K. Esfarjani, G. Chen, and H. T. Stokes, Phys. Rev. B **84**, 085204 (2011).

[17] P. Giannozzi, S. de Gironcoli, P. Pavone, and S. Baroni, Phys. Rev. B **43**, 7231 (1991).

[18] S. Baroni, S. de Gironcoli, A. Dal Corso, and P. Giannozzi, Rev. Mod. Phys. **73**, 515 (2001).

[19] J. P. McKilvey, *Solid State and Semiconductor Physics (International Edition)* (Harper and Row, New York, Evanston, London, and John Weatherhill Inc., Tokyo, 1966).

[20] J. S. Blakemore, *Solid State Physics* (W. B. Saunders Company, Philadelphia, 1970), p. 262.

[21] J. R. Drabble and H. J. Goldsmit, *Thermal Conduction in Semiconductors* (Pergamon, Oxford, 1961).

[22] B. R. Nag, *Theory of Electrical Transport in Semiconductors* (Pergamon, Oxford, 1972).

[23] J. Yang in *Thermal Conductivity: Theory, Properties and Applications*, edited by T. M. Tritt (Kulwer/Plenum, New York, Boston, Dordrecht, London, Moscow, 2004), p. 1.

[24] P. J. Price, Philos. Mag. Series 7 **46**, 1252 (1955).

[25] G. A. Slack and C. Glassbrenner, Phys. Rev. **120**, 782 (1960); C. J. Glassbrenner and G. A. Slack, *ibid.* **134**, A1058 (1964).

[26] G. P. Srivastava, *The Physics of Phonons* (Adam Hilger, Bristol, 1990).

[27] P. Carruthers, Rev. Mod. Phys. **33**, 92 (1961).

[28] G. A. Slack, Phys. Rev. **105**, 829 (1957).

[29] G. A. Slack, Phys. Rev. **126**, 427 (1962).

[30] T. H. Geball and G. W. Hull, Phys. Rev. **110**, 773 (1958).

[31] *CRC Handbook of Chemistry and Physics*, edited by R. C. Weast, 58th ed. (CRC Press, Florida, 1977), p. B-274.

[32] G. Deinzer, G. Birner, and D. Strauch, Phys. Rev. B **67**, 144304 (2003).

[33] K. Esfarjani and H. T. Stokes, Phys. Rev. B **77**, 144112 (2008).

[34] M. Lopuszyński and J. A. Majewski, Phys. Rev. B **76**, 045202 (2007).

[35] *Landolt-Börnstein Numerical Data and Functional Relationships in Science and Technology: Group III*, edited by O. Madelung, M. Schulz, and H. Weiss (Springer-Verlag, Berlin, Heidelberg, New York, 1982), Vol. 17a.

[36] G. A. Slack and S. F. Bartram, J. Appl. Phys. **46**, 89 (1975).

[37] A. Ward and D. A. Broido, Phys. Rev. B **81**, 085205 (2010).

[38] J. M. Ziman, *Electrons and Phonons* (Oxford University Press, Oxford, New York, 1967).

[39] A. AlShaikhi and G. P. Srivastava, Phys. Rev. B **76**, 195205 (2007).

[40] S. P. Hepplestone and G. P. Srivastava, Phys. Rev. B **84**, 115326 (2011).

[41] J. M. Sze, *Physics of Semiconductor Devices*, 2nd ed. (Wiley, New York, Chichester, Brisbane, Toronto, Singapore, 1981), p. 15.

[42] H. J. Monkhorst and J. D. Pack, Phys. Rev. B **13**, 5188 (1976).

[43] P. Gianozzi *et al.*, J. Phys. Cond. Mat. **21**, 395502 (2009); code available from [http://www.quantum-espresso.org].

[44] To be specific, we used the pseudopotentials Si.pz-vbc.UPF and Ge.pz-bhs.UPF, which are available from [http://www.quantum-espresso.org].

[45] W. H. Press, B. P. Flanney, S. A. Teukolsky, and W. T. Vetterling, *Numerical Recipies: The Art of Scientific Computing* (Cambridge University Press, Cambridge, 1986), pp. 521–528.

[46] O. C. Yelgel and G. P. Srivastava, Phys. Rev. B **85**, 125207 (2012).

[47] A. Kokalj, J. Mol. Graphics Modell. **17**, 176 (1999); Comput. Mater. Sci. **28**, 155 (2003); code available from [http://www.xcrysden.org/].

[48] S. P. Hepplestone and G. P. Srivastava, Phys. Rev. Lett. **101**, 105502 (2008).

[49] S. P. Hepplestone and G. P. Srivastava, J. Appl. Phys. **107**, 043504 (2010).

[50] W. Fon, K. C. Schwab, J. M. Worlock, and M. L. Roukes, Phys. Rev. B **66**, 045302 (2002).

[51] A. J. Minnich, J. A. Johnson, A. J. Schmidt, K. Esfarjani, M. S. Dresselhaus, K. A. Nelson, and G. Chen, Phys. Rev. Lett. **107**, 095901 (2011).

[52] R. A. Richardson, S. D. Peacor, C. Uher, and Franco Nori, J. Appl. Phys. **72**, 4788 (1992).

[53] P. G. Klemens, Phys. Rev. **148**, 845 (1966).

[54] B. K. Ridley and R. Gupta, Phys. Rev. B **43**, 4939 (1991).

[55] Unpublished. In fact, this appendix is our reconstruction of his probable reasoning, which is currently unavailable to us.

[56] P. G. Klemens in *Solid State Physics*, edited by F. Seitz and D. Turnbull (Academic Press, New York, 1958), Vol. 7, p. 1; P. G. Klemens, Phys. Rev. **122**, 443 (1961).